Atmospheric
Chemistry
and Physics

Open Access

Isoprene emissions over Asia 1979–2012: impact of climate and land-use changes

T. Stavrakou[1], **J.-F. Müller**[1], **M. Bauwens**[1], **I. De Smedt**[1], **M. Van Roozendael**[1], **A. Guenther**[2,*], **M. Wild**[3], and **X. Xia**[4]

[1]Belgian Institute for Space Aeronomy, Avenue Circulaire 3, 1180, Brussels, Belgium
[2]Atmospheric Chemistry Division, National Center for Atmospheric Research, 1850 Table Mesa Drive, Boulder, Colorado, 80305, USA
[3]Institute for Atmospheric and Climate Science, ETH Zurich, Universitaetsstr. 16, 8092 Zurich, Switzerland
[4]LAGEO, Institute for Atmospheric Physics, Chinese Academy of Sciences, Beijing, China
[*]now at: Atmospheric Sciences and Global Change Division, Pacific Northwest National Laboratory, Richland, Washington State, USA

Correspondence to: T. Stavrakou (jenny@aeronomie.be)

Abstract. Due to the scarcity of observational constraints and the rapidly changing environment in East and Southeast Asia, isoprene emissions predicted by models are expected to bear substantial uncertainties. The aim of this study is to improve upon the existing bottom-up estimates, and to investigate the temporal evolution of the fluxes in Asia over 1979–2012. To this purpose, we calculate the hourly emissions at $0.5° \times 0.5°$ resolution using the MEGAN–MOHYCAN model driven by ECMWF ERA-Interim climatology. In order to remedy for known biases identified in previous studies, and to improve the simulation of interannual variability and trends in emissions, this study incorporates (i) changes in land use, including the rapid expansion of oil palms, (ii) meteorological variability according to ERA-Interim, (iii) long-term changes in solar radiation (dimming/brightening) constrained by surface network radiation measurements, and (iv) recent experimental evidence that South Asian tropical forests are much weaker isoprene emitters than previously assumed, and on the other hand, that oil palms have a strong isoprene emission capacity. These effects lead to a significant lowering (factor of 2) in the total isoprene fluxes over the studied domain, and to emission reductions reaching a factor of 3.5 in Southeast Asia. The bottom-up annual isoprene emissions for 2005 are estimated at 7.0, 4.8, 8.3, and 2.9 Tg in China, India, Indonesia and Malaysia, respectively. The isoprene flux anomaly over the whole domain and studied period is found to be strongly correlated with the Oceanic

Niño Index ($r = 0.73$), with positive (negative) anomalies related to El Niño (La Niña) years.

Changes in temperature and solar radiation are the major drivers of the interannual variability and trends in the emissions, except over semi-arid areas such as northwestern China, Pakistan and Kazakhstan, where soil moisture is by far the main cause of interannual emission changes. In our base simulation, annual positive flux trends of 0.2 % and 0.52 % throughout the entire period are found in Asia and China, respectively, related to a positive trend in temperature and solar radiation. The impact of oil palm expansion in Indonesia and Malaysia is to enhance the trends over that region, e.g., from 1.17 % to 1.5 % in 1979–2005 in Malaysia. A negative emission trend is derived in India (−0.4 %), owing to the negative trend in solar radiation data associated with the strong dimming effect likely due to increasing aerosol loadings.

The bottom-up emissions are compared to field campaign measurements in Borneo and South China and further evaluated against top-down isoprene emission estimates constrained by GOME-2/MetOp-A formaldehyde columns through 2007–2012. The satellite-based estimates appear to support our assumptions, and confirm the lower emission rate in tropical forests of Indonesia and Malaysia. Additional flux measurements are clearly needed to characterize the spatial variability of emission factors better. Finally, a decreasing trend in the inferred top-down Chinese emissions since 2007

is in line with recorded cooling in China after that year, thus suggesting that the satellite HCHO columns are able to capture climate-induced changes in emissions.

---

1 Introduction

Isoprene is a key tropospheric species, well known as the dominant biogenic hydrocarbon emitted into the atmosphere, with global annual emissions of 400–600 Tg (Guenther et al., 2006). It is highly reactive, believed to enhance tropospheric ozone formation in polluted conditions and to contribute to secondary aerosol formation (Claeys et al., 2004), yet its degradation in the atmosphere, especially in pristine environments, is still not fully understood (Lelieveld et al., 2008; Peeters and Müller, 2010; Crounse et al., 2011). The emissions of isoprene and other biogenic VOCs are primarily dependent on the nature and abundance of plants, as estimated by indicators such as the basal emission rate (BER) and the leaf area index (LAI). They are further modulated by meteorological parameters. Both climate and land-use changes can therefore influence the spatiotemporal and interannual variability of the emissions. Besides these factors, the increasing CO_2 concentration might influence the productivity of vegetation and the isoprene emission rates, but such effects bear large uncertainties (Arneth et al., 2007; Heald et al., 2009; Lathière et al., 2010; Guenther et al., 2012).

Incorporating a large number of available isoprene flux measurements, the Model of Emissions of Gases and Aerosols from Nature (MEGAN) emission model (Guenther et al., 2006), enables the calculation of isoprene fluxes using state-of-the-art distribution of BER, and response functions for the effects of temperature, solar radiation, soil moisture, leaf age and leaf area index. However, MEGAN is based on isoprene flux observations available on a sparse spatiotemporal network; their extrapolation is expected to be prone to substantial uncertainties due to the high variability of the isoprene emission fluxes. In particular, the available observational constraints incorporated in MEGAN for Asian ecosystems are very limited. A better characterization of isoprene emission is required, especially since East and Southeast Asia experienced substantial increases in anthropogenic emissions of ozone precursors and aerosols in the last two decades (e.g., Richter et al., 2005; Stavrakou et al., 2008; Kurokawa et al., 2013), related to the rapidly expanding economic activity. Moreover, Southeast Asia faced massive land-use changes during the last decades, in particular deforestation and conversion of primary forests to croplands, often leading to a decrease in isoprene fluxes, since crops are generally known to be weaker isoprene emitters than the forests they substitute (Guenther et al., 2006). The conversion of land to oil palm plantations in Indonesia and Malaysia is a particular case of land-use change. The expansion of oil palm plantation areas has been extremely rapid between 1979

and 2010: a factor of 20 in Indonesia, and a factor of 55 in the State of Sarawak in Borneo (Miettinen et al., 2012a, b). Crops in China are being converted to tree plantations (e.g., eucalyptus and rubber trees) for economic reasons, resulting in large increases in isoprene fluxes (Geron et al., 2006).

Next to land use, solar radiation is a key driver of isoprene fluxes. However, the ECMWF reanalysis fields fail to capture observed surface radiation data, especially at Chinese sites (Wild and Schmucki, 2010), most likely because changes in the aerosol loading and composition are entirely omitted in the ECMWF analyses. Significant dimming and brightening have been observed over Asia in the last decades, in particular in eastern China and India (Xia, 2010; Padma Kumari et al., 2007; Wild, 2009). More specifically, a strong solar dimming was observed in China from 1961 to 1990, especially over eastern China, where surface stations recorded negative trends of about $10\,W\,m^{-2}$ per decade. This tendency slowed down after 1990 in northern China, and even changed sign in southern China (Xia, 2010). Whereas the solar dimming observed before 1990 appeared to be only weakly related to cloud cover changes, the positive solar flux trend over 1990–2002 was found to be partly due to reductions in cloud cover (Norris and Wild, 2009). The same study reported a slight decrease in solar fluxes over Japan ($-1\,W\,m^{-2}$ per decade) during 1971–1989, and a significant brightening ($8\,W\,m^{-2}$ per decade) over 1990–2002, partly explained by reductions in the cloud coverage (Norris and Wild, 2009). However, this brightening was observed to level off in Japan between 2000 and 2005, providing an indication of changes similar to those observed in China (Wild et al., 2009; Xia, 2010).

In India, solar radiation data showed an average solar dimming of $8.6\,W\,m^{-2}$ per decade between 1981 and 2004 (Padma Kumari et al., 2007), similar to the trend observed between 2000 and 2005 ($-11\,W\,m^{-2}$ per decade, Wild et al., 2009). This trend is believed to be due to rapidly increasing emissions of aerosol (and aerosol precursors) (Padma Kumari et al., 2007; Ramanathan and Carmichael, 2008). Finally, in addition to the poor representation of solar radiation trends in ECMWF analyses, a recent study reported that ERA-Interim overestimates downward solar radiation fields by 8–20 % in comparison to ground observations at a large number of stations over China (Jia et al., 2013).

Deforestation in Southeast Asia is expected to cause significant changes in isoprene emissions. Their estimation is uncertain due to possible errors in the emission capacities for both natural forests and managed landscapes. Recent field measurements obtained in northern Borneo during the OP3 field campaign (Langford et al., 2010; Fowler et al., 2011), and in a tropical forest in Peninsular Malaysia (Saito et al., 2008) indicated that MEGAN overestimates the isoprene emission capacity of primary tropical forests in this region, and possibly more generally in South Asia. The low basal emission rate inferred for natural forests by Langford et al. (2010) ($1.65\,mg\,m^{-2}\,h^{-1}$) and by Saito et al. (2008)

(1.2 mg m^{-2} h^{-1}) is higher than the very low emission capacities assumed for most crops and pasture (≤ 1 mg m^{-2} h^{-1}) (Guenther et al., 2006) and much lower than the very high emission rate (~ 10 mg m^{-2} h^{-1}) due to oil palms (Misztal et al., 2011; Hewitt et al., 2011). It is therefore necessary to account for both the expansion of oil palm plantations and the expansion of other crops in order to determine the effects of deforestation on emissions in South Asia. In order to quantify the isoprene emissions over Asia and their temporal evolution through 1979–2012 better, we use the MEGAN model coupled with the MOdel of HYdrocarbon emissions by the CANopy (MOHYCAN) model (Müller et al., 2008), with several important updates: the incorporation of changes in land use (Ramankutty and Foley, 1999), the explicit consideration of oil palm emissions following the algorithm of Misztal et al. (2011), and the incorporation of corrections in ECMWF solar radiation fields based on surface solar radiation data (Wild et al., 2009; Xia, 2010). The resulting bottom-up inventory is evaluated against field measurements and top-down isoprene flux estimates over 2007–2012 derived by inverse modeling using a global CTM constrained by GOME-2 formaldehyde (HCHO) columns.

Section 2 provides a short description of the MEGAN–MOHYCAN model and presents the performed simulations (S0–S4). The variability and trends of the isoprene emissions through 1979–2012 derived from the standard model run are discussed in Sect. 3, whereas the isoprene fluxes derived across all simulations are discussed in detail in Sect. 4 and on a country-by-country basis in Sect. 5. In Sect. 6 we present comparisons with ground-based measurements in Borneo and South China. The IMAGESv2 chemistry-transport model, the GOME-2 satellite data and the inversion setup are briefly presented in Sect. 7, and a comparison of the bottom-up with top-down emission results is presented in Sect. 7.2. Conclusions are drawn in Sect. 8.

2 Model description and simulations

2.1 MEGAN coupled with MOHYCAN canopy model

The MEGAN isoprene emission model for isoprene has been thoroughly described in Guenther et al. (2006) and in numerous studies, and therefore it will be only briefly discussed here. The algorithm includes the specification of a standard emission factor (ϵ, mg m^{-2} h^{-1}), also termed emission capacity, representing the emission in standard conditions (Guenther et al., 2006). The activity factor (γ) accounts for the response of the emission on leaf-level temperature, and solar radiation, as well as on leaf age, soil moisture, and the leaf area index (LAI). Leaf temperature and light attenuation by the canopy are calculated by the MOHYCAN canopy environment model (Müller et al., 2008). More specifically, the net flux rate above the canopy is given by

$$F = \epsilon \cdot \gamma, \text{ in mg m}^{-2} \text{ h}^{-1} \tag{1}$$

$$\gamma = 0.52 \cdot \gamma_{\text{age}} \cdot \gamma_{\text{SMS}} \cdot \sum_{j=1}^{8} \sum_{i=1}^{2} [(\gamma_P)_i^j \cdot (\gamma_T)_i^j \cdot f_i^j)] \cdot \text{LAI}_j \tag{2}$$

where i runs over sun and shade leaves, j over the eight canopy layers of the MOHYCAN model, γ_{age}, and γ_{SMS} are the leaf age and soil moisture stress activity factors, LAI_j the LAI at layer j, f^j the fraction of sun or shade leaves at layer j, and γ_T, γ_P the activity factors expressing the response of emissions to leaf temperature and photosynthetic photon flux density (P, in µg mol m^{-2} s^{-1}), respectively. The dependence on light is expressed as

$$\gamma_P = C_P \cdot \alpha \cdot P \cdot (1 + \alpha^2 \cdot P^2)^{-1/2}, \tag{3}$$

with $C_P = 0.0468 \cdot \exp(0.0005 \cdot (P_{24} - P_0)) \cdot (P_{240})^{0.6}$, $\alpha = 0.004 - 0.0005 \cdot \ln(P_{240})$, where P in Eq. (3) is calculated at leaf level, P_0 is set to 200 or 50 µg mol m^{-2} s^{-1} for sun or shade leaves, respectively, whereas P_{24} and P_{240} are averages of light intensity over the last 24 and 240 h. The dependence on temperature is parameterized by the formula

$$\gamma_T = \frac{E_{\text{opt}} \cdot C_{T2} \cdot e^{C_{T1} \cdot A}}{C_{T2} - (C_{T1} \cdot (1 - e^{C_{T2} \cdot A}))}, \quad A = \frac{T_\ell - T_{\text{opt}}}{R \cdot T_\ell \cdot T_{\text{opt}}} \tag{4}$$

with $C_{T1} = 95 \times 10^3$ J mol^{-1}, $C_{T2} = 23 \times 10^4$ J mol^{-1}, T_ℓ is the leaf temperature determined by MOHYCAN, R is the universal gas constant, and E_{opt} is defined as a function of the average leaf temperature (K) over the last 24 and 240 h (T_{24}, T_{240}):

$$E_{\text{opt}} = 2.034 \cdot e^{0.05(T_{24} - 297)} \cdot e^{0.05(T_{240} - 297)} \tag{5}$$

$$T_{\text{opt}} = 313 + 0.6 \cdot (T_{240} - 297). \tag{6}$$

The emission response to leaf age is defined as

$$\gamma_{\text{age}} = 0.05 \cdot F_1 + 0.6 \cdot F_2 + 1.125 \cdot F_3 + F_4, \tag{7}$$

where F_1, F_2, F_3, F_4 are the fractions of new, growing, mature, and senescent leaves, respectively (Guenther et al., 2006). The dependence on soil moisture stress is estimated from the soil water content and the wilting point (Müller et al., 2008).

Six plant functional types (broadleaf trees, needleleaf evergreen/deciduous trees, shrub, grass, crops) are considered (Guenther et al., 2006), and the global distribution of the basal emission factor ϵ for each of the above plant functional types (Eq. 1) is obtained at a resolution of 0.5° × 0.5° from MEGAN EF version 2011.

The MOHYCAN canopy model is used to determine the leaf temperature and radiation fluxes as a function of the height in the canopy, using visible and near-infrared solar

radiation values at the canopy top, together with air temperature, relative humidity, wind speed and cloud cover. This is realized by (i) estimating the direct and diffuse fractions of solar radiation at each of the eight MOHYCAN canopy levels using the radiative transfer model of Goudriaan and Laar (1994); Leuning et al. (1995), (ii) determining leaf temperature iteratively using the energy balance equation (Goudriaan and Laar, 1994; Leuning et al., 1995) by including the determination of resistances for the exchange of heat and water vapour between the air and the leaves, and accounting for attenuation of the wind speed by the foliage, as detailed in Müller et al. (2008). Direct and diffuse fractions of solar radiation at canopy top depend on solar zenith angle and cloud optical depth. The latter is estimated from the downward visible solar radiation flux (P) based on tabulated irradiances calculated using the TUV (Tropospheric Ultraviolet and Visible, Madronich and Flocke, 1998) atmospheric radiative transfer model.

ERA-Interim operational meteorological fields for the period between 1979 and 2012 are used to drive the MOHYCAN and MEGAN models. More specifically, downward solar radiation, cloud cover fraction, volumetric soil moisture at four soil layers, above-surface air temperature, dewpoint temperature, and wind speed directly above the canopy are provided every 6 h and re-gridded at a resolution of $0.5° \times 0.5°$. The emissions are calculated for both clear sky and cloudy conditions using cloud optical depth estimated using the cloud cover fraction and the tabulated solar radiation irradiances. Assuming cloud cover and cloud optical depth to be constant in each 6 h interval, hourly values of diffuse and direct solar radiation fluxes are derived under both clear sky and cloudy conditions, using the above TUV model.

Leaf area index data are obtained from the collection 5 MODIS 8-day MOD15A2 composite product generated by using daily Aqua and Terra observations at $1 \, km^2$ resolution, and can be accessed via the MODIS site (ftp://e4ftl01.cr.usgs.gov/MOTA/MCD15A2.005) for all years between 2003 and 2012, whereas monthly climatological LAI values derived from the same data set are used before 2002.

2.2 Description of the simulations

Five simulations, covering the domain 9.75° S–54.75° N and 60.25–149.75° E, are performed and summarized in Table 1. The baseline simulation (S0) uses the MEGAN–MOHYCAN model described in the previous section and covers the period 1979–2012. This simulation accounts for the effects of climate change according to ERA-Interim data. In simulation S1, the static land-use cropland map used in MEGAN is replaced by the vegetation map of Ramankutty and Foley (1999) to account for the effect of land-use changes. The updated version of the historical cropland data set (http://www.geog.mcgill.ca/~nramankutty/Datasets/Datasets.html) provides the annual global distribution of the cropland fraction at a resolution of 0.5° and spans the pe-

riod from 1700 to 2007. A rapid cropland increase is suggested in Southeast Asia between 1979 and 2007, often associated with large-scale deforestation, whereas significant cropland abandonment is found to be widespread in central and southern China, mostly due to urbanization. The largest increases in cropland fraction between 1979 and 2007 occurred in Indonesia (1.5 % yr^{-1}), Malaysia (2.3 % yr^{-1}), and Laos–Vietnam–Cambodia (3 % yr^{-1}) (Fig. 1).

The S2 simulation accounts for the recent evidence that emissions of isoprene over primary tropical forests are likely to be largely overestimated in the MEGAN model in Southeast Asia, by as much as a factor of 4.1 in comparison to above-canopy flux measurements in Borneo (Langford et al., 2010). This factor is applied to the MEGAN emission rate for all (primary) tropical forests in the S2 scenario.

In the S3 case we consider the impact of oil palm expansion in regions experiencing rapid expansion of plantations, like Indonesia and Malaysia. To that effect, we introduce an additional plant functional type for oil palm and use the modified MEGAN emission model developed by Misztal et al. (2011) and optimized using canopy-scale measurements over an oil palm plantation in northern Borneo. This parameterization uses a basal emission rate of $22.8 \, mg \, m^{-2} \, h^{-1}$. Note that, over Malaysia, the S0 simulation already accounts for the presence of oil palm, as reflected by increased basal emission rates (3–$4 \, mg \, m^{-2} \, h^{-1}$) for the cropland PFT over this country. In S3, the basal emission rate of croplands (excluding oil palm) over Malaysia was set to $0.8 \, mg \, m^{-2} \, h^{-1}$, comparable to values found over Indonesia in MEGAN.

The spatial distribution of oil palm plantation is obtained from a 250 m-resolution composite land cover map of insular Southeast Asia derived from daily surface reflectance MODIS data for 2010 (Koh et al., 2011; Miettinen et al., 2012a). The map, which covers Malaysia and Indonesia, has been gridded onto the 0.5° resolution (Fig. 2). The evolution of oil palm planted areas between 1979 and 2010 for Indonesia is obtained from Miettinen et al. (2012b) and for Malaysia from statistical data for mature palms (trees above 3 years old and bearing fruits, http://bepi.mpob.gov.my). The planted area expanded extremely rapidly between 1979 and 2010, especially in the Malaysian state of Sarawak, where it increased by a factor of 55, as well as in Indonesia and Sabah (factor of 20, Fig. 2).

The S4 experiment is designed to account for decadal changes in solar radiation fields observed in Asian regions, which the ECMWF analyses cannot reproduce due to their static representation of aerosols. To this purpose, we use annual surface solar radiation anomaly data observed at several stations in China from Xia (2010) between 1979 and 2005, and over Japan and India from Wild and Schmucki (2010) until 2000, extrapolated until 2005 based on Wild et al. (2009) (Fig. 3). ECMWF solar radiation data have been used to calculate the annually averaged solar radiation (SSR_{ECMWF}) at the locations of the observation sites, and their average over 1979–2005 ($\overline{SSR}_{ECMWF}$), and to derive
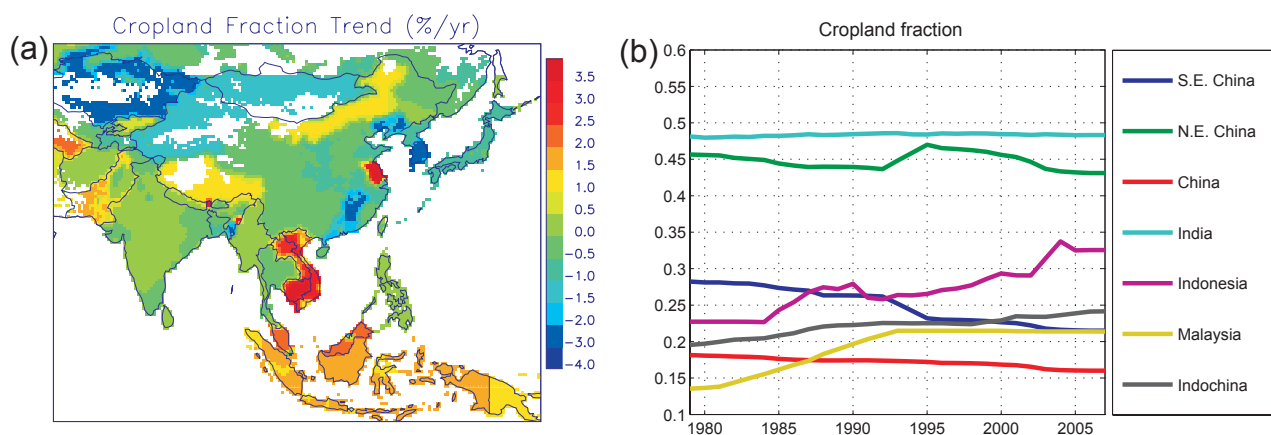
Fig. 1. (a) Trend distribution of cropland fraction between 1979 and 2007. **(b)** Evolution of cropland fraction per country between 1979 and 2007. *Source:* Ramankutty and Foley (1999) and updates (http://www.geog.mcgill.ca/~nramankutty/Datasets/Datasets.html).
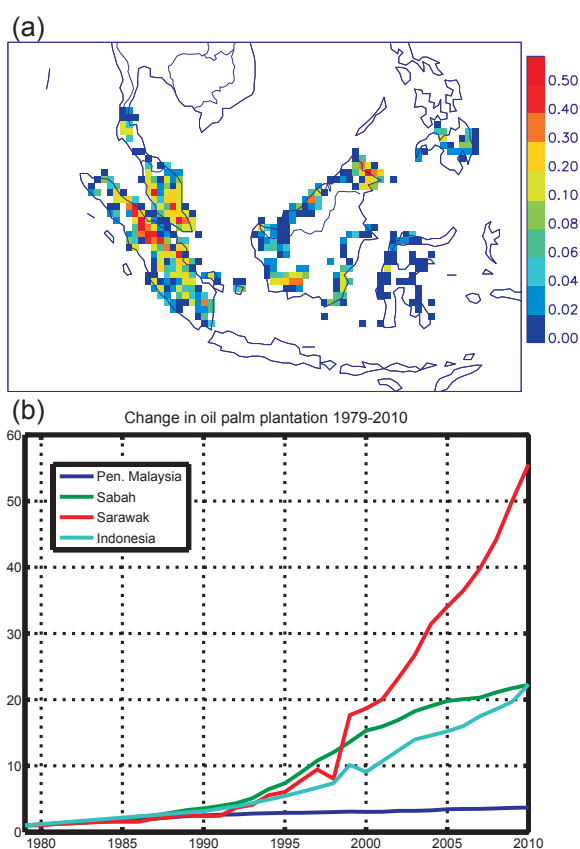

Fig. 2. (a) Spatial distribution of the fraction of oil palm plantations in 2010 (Koh et al., 2011; Miettinen et al., 2012a) gridded onto 0.5° resolution. **(b)** Evolution of oil palm plantation area in Indonesia and Malaysia (Peninsular Malaysia, Sabah, and Sarawak) between 1979 and 2010, normalized to the 1979 value. *Source:* Miettinen et al. (2012b) for Indonesia, http://bepi.mpob.gov.my for Malaysia.

radiation correction factors c_i defined as

$$c_i = \frac{\overline{SSR}^i_{ECMWF} + \Delta(SSR^i_{obs})}{\overline{SSR}^i_{ECMWF} + \Delta(SSR^i_{ECMWF})} \qquad (8)$$

where i denotes five regions comprising observation locations (Wild and Schmucki, 2010; Xia, 2010), namely northeastern China (32.75–47.75° N, 108.25–130.75° E, 13 sites), southeastern China (18.25–32.25° N, 109.75–122.75° E, 12 sites), southwestern China (22.25–32.25° N, 96.25–109.25° E, 8 sites), Japan (31.25–41.75° N, 130.25–144.75° E, 25 sites) and India (5.25–29.75° N, 70.25–89.75° E, 4 sites). In Eq. (8), $\Delta(SSR_{obs})$ stands for the annual observed anomaly of solar radiation data averaged over the regions i, and

$$\Delta(SSR_{ECMWF}) = SSR_{ECMWF} - \overline{SSR}_{ECMWF} \qquad (9)$$

the corresponding anomaly in the ECMWF data. The correction factors c_i are calculated for every year between 1979 and 2005, and are uniformly applied to the photosynthetic photon flux density (P) in each region (Fig. 3).

Furthermore, S4 accounts for the results obtained from a recent evaluation of the ERA-Interim downward radiation fields over China, revealing a systematic overestimation in the ERA-Interim data set, by 8.4 % in northeastern China (42–54° N, 120–132° E), by 13.7 % in western China (32–48° N, 85–100° E), 14.4 % in northern China (32–44° N, 100–120° E), and by 20.2 % in southern China (18–32° N, 100–122° E) (Jia et al., 2013). As previously, these correction factors are applied to the photosynthetic photon flux density (P) in each of these regions.

3 Variability and trends in isoprene emissions

Figure 4 displays the distribution of the correlation coefficient between annual isoprene emissions in the S0 simulation and the main meteorological drivers of the emission,

Table 1. Scenarios for calculating isoprene emissions.

| Name	Description	Period
S0	MEGAN–MOHYCAN, standard settings	1979–2012
S1	As S0, accounts for land-use changes (Ramankutty and Foley, 1999)	1979–2007
S2	As S1, emission factor reduction for tropical forests	1979–2007
S3	As S2, accounts for changing oil palm distribution in Indonesia and Malaysia	1979–2007
S4	As S3, correct solar radiation based on network of observations	1979–2005
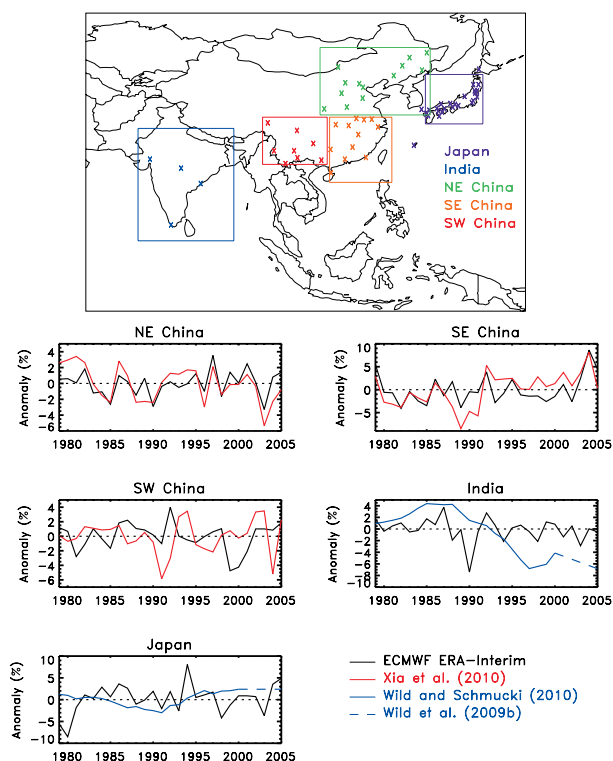
Fig. 3. Upper panel: the crosses represent the locations of surface radiation measurement stations in China, Japan and India, as reported in Xia (2010); Wild and Schmucki (2010). Lower panel: annual downward surface solar radiation (SSR) anomaly (in %) derived from ERA-Interim fields (black) and corrected based on ground-based SSR observations in China (Xia, 2010), India and Japan (Wild and Schmucki, 2010; Wild et al., 2009).

namely air temperature, above-canopy radiation and the soil moisture stress activity factor. Unsurprisingly, the calculated emissions are strongly correlated with PAR levels over most non-arid regions, and especially over forested areas. This is a consequence of both the direct effect of PAR on emissions (Eq. 2) and the indirect effect through the temperature activity factor (Eq. 4) and the dependence of leaf temperature on solar radiation (Müller et al., 2008). Compared to PAR, air temperature is less well correlated with the emissions in many regions, in part because it is leaf temperature, not air temperature, which drives the temperature activity fac-

tor. Furthermore, at extratropical latitudes, the emissions are likely better correlated with summertime temperature than with annual temperature, since most of the annual emissions take place during the summer. Over arid and semi-arid regions, soil moisture is clearly the main meteorological driver of interannual variability. Negative correlation coefficients between the emissions and the soil moisture activity factor over, e.g., eastern China result from the correlation of soil moisture with cloudiness, which is itself anticorrelated with PAR. The same effect also explains the negative correlations between emission and PAR over arid areas.

The spatial distribution of the 1979–2012 trends in isoprene emissions (as estimated by the standard S0 simulation) are generally well explained by the distribution of trends in temperature and radiation and the soil moisture activity factor (Fig. 5). Over non-arid areas, temperature and radiation dominate the behavior of the resulting flux. Over Kazakhstan, Pakistan, western India and northwestern China, however, positive trends in emissions are primarily caused by increasing trends in soil moisture in those areas. The interannual variation of the emissions for the entire simulation period (1979–2012) is illustrated in Fig. 6. The emission fluxes exhibit strong year-to-year variations, and a positive trend throughout the whole period. To ease the interpretation of the results, we display in the same figure the ERA-Interim mean annual temperature and photosynthetically active radiation (PAR) over the whole studied domain and over China.

China experiences a large isoprene flux trend, amounting to $0.52\,\%\,\mathrm{yr}^{-1}$, over 1979–2012. The primary drivers for this trend are the apparent warming rate ($0.3\,^{\circ}\mathrm{C}\,\mathrm{decade}^{-1}$) and the increasing solar radiation trend ($0.3\,\%\,\mathrm{decade}^{-1}$). The region experiencing the strongest warming trend (0.4–$0.6\,^{\circ}\mathrm{C}$ per decade) is situated close to Shanghai (Jiangsu, Anhui, and Zhejiang provinces), as well as in the northern provinces, in agreement with reported data from a large number of weather stations in China (Liu et al., 2004). In southern China, however, the decadal temperature trend is generally lower than $0.4\,^{\circ}\mathrm{C}$ per decade and often close to zero, but the radiation trend is larger in this region (1–$3\,\%\,\mathrm{decade}^{-1}$). The isoprene emission trend in northern Borneo is strongly positive ($3\,\%\,\mathrm{yr}^{-1}$), owing to the combined effect of the positive trends in temperature and in solar radiation, whereas emission decreases are found elsewhere in Malaysia and Indonesia, primarily due to the decreasing trend in solar radiation

(Fig. 5). The largest isoprene trends are found at the frontier between Mongolia, China, and Russia, but it should be noted that the isoprene emitting capacity is rather weak in those regions (cf. Sect. 4).

Over China, the largest emission flux is calculated in 2007, the warmest year in our data series, but also a year experiencing high values of solar radiation (Fig. 6). Between 2008 and 2012, however, the mean annual temperature declined, resulting in decreasing isoprene fluxes for these years. The total emissions in the Asian domain were highest in 1997 and 1998, as a consequence of the exceptionally strong El Niño event affecting Southeast Asia. As illustrated in Fig. 6, radiation fluxes were highest in 1997, whereas in 1998 the mean annual temperature was among the highest ever recorded in the domain. The lowest isoprene emission is computed in 2008, mostly due to low temperatures and high cloud cover associated with the strong La Niña episode affecting Southeast Asia. The trend in the mean temperature over the entire period and domain is positive ($0.24\,^\circ$C per decade), whereas the radiation undergoes a slightly negative trend.

Comparison of the isoprene flux anomaly, i.e., an anomaly with respect to the 1979–2012 mean, over the whole domain with the Oceanic Niño Index (ONI), defined as the running 3-month mean sea surface temperature anomaly for the region 5° N–5° S, 120–170° W, reveals a strong correlation (0.73) over the whole period, as illustrated in Fig. 7. In particular, negative deviations are related to weak (1984–1985), medium (2007–2008), or strong (1988–1989, 1999) La Niña years, whereas opposite deviations correspond to medium (1987, 2009–2010) and strong (1997–1998) El Niño episodes. This result is in qualitative agreement with findings from past studies reporting that global biogenic emissions are generally higher during El Niño and lower during La Niña years due to the strong influence of warming and cooling oceanic cycles (Naik et al., 2004; Lathière et al., 2006). In our comparison (Fig. 7), ONI is lagged by 3 months, to account for a possible delay in the effects of the El Niño/La Niña, yet the correlation coefficient is also very high for the whole domain (0.64) even without assuming any shift in the ONI index. The lagged ONI is found to be only weakly correlated with isoprene emissions from China (0.24).

In order to assess the possible role of LAI interannual variability in isoprene emissions, we compare the trends in our base emissions between 2002 and 2012 (i.e., using LAI varying from year to year) with emission trends calculated using climatological LAI during the same period. The emission trends are almost unaffected over the whole domain (e.g., -0.221 and $0.237\,\%\,\text{yr}^{-1}$ using variable or climatological LAI, respectively) or in Southeast Asia (e.g., 0.148 and $0.160\,\%\,\text{yr}^{-1}$ over Indonesia). Larger changes are found over more arid areas such as western India and northwestern China (e.g., 0.796 and $0.439\,\%\,\text{yr}^{-1}$ over India). Noting that these regions are characterized by low LAI values (typically < 1.5) for which the MODIS-based estimations are expected

to be very uncertain, we conclude that the impact of LAI interannual variability is generally either small or uncertain.

The increasing trend in CO_2 concentrations might have a significant impact on isoprene emission (Arneth et al., 2007). Using the simple parameterization proposed by Heald et al. (2009), based on the observed long-term response of isoprene to CO_2 changes for aspen trees, the CO_2 increase between 1979 (337 ppmv) and 2012 (394 ppmv) is estimated to induce a decrease of ca. 5 % in the isoprene emission, corresponding to a negative trend of $0.15\,\%\,\text{yr}^{-1}$. Although significant compared to the trends associated with climate change, it has been ignored here due to its high uncertainty, and because it is not a significant driver of interannual variability.

4 Isoprene fluxes across S0–S4 simulations

The annual isoprene emission distributions calculated by the different simulations (Table 1) are illustrated in Fig. 8 in 2005. The total annual flux estimated by the standard S0 run amounts to 90.4 Tg (Table 2) and originates mostly in the dense tropical ecosystems prevailing between 10 and 20° N. Two countries, Indonesia and Malaysia, are responsible for about 40 % of the total emission in the studied domain in the S0 simulation. In China, the highest emission rates are found in the southeastern part, whereas emissions in the northeast are limited by virtue of the lower temperatures and near-zero emission during wintertime from deciduous trees, dominant in this region.

The replacement of the cropland database in the S1 experiment leads to generally lower isoprene emissions, because of the larger cropland fraction in the Ramankutty and Foley (1999) distribution (Fig. 1) and the fact that crops are weak isoprene emitters. This decrease is consistent with previously estimated isoprene emission decreases due to the conversion of forested land to cropland (Steiner et al., 2002; Tanaka et al., 2012; Wu et al., 2012). The fluxes in 2005 decrease by 17 % in Malaysia, by 27 % in India, and by 40 % in Indonesia, whereas they are slightly increased in China (by 6 %), as a result of the cropland abandonment suggested by the land-use change database in the southeastern part of the country.

As expected given the importance of tropical forests in South Asia, the strong reduction in their emission rates adopted in S2 (and subsequent) simulations induces the most significant change in the calculated emissions. The emission reduction over the whole domain amounts to a factor of 2 compared to the standard simulation (Table 2), and is even higher in the case of Malaysia and Indonesia, where the reductions are the largest, by factors of 2.7 and 4, respectively.

The explicit consideration of oil palm plantations in the S3 scenario results in a 10 % increase in isoprene fluxes in Indonesia in 2005. The increase is most significant in northern Sumatra and southern Borneo, which are to a large extent ($\sim 50\,\%$) covered by oil palms (Fig. 2). While Indonesian emissions are increased, a slight decrease is found for
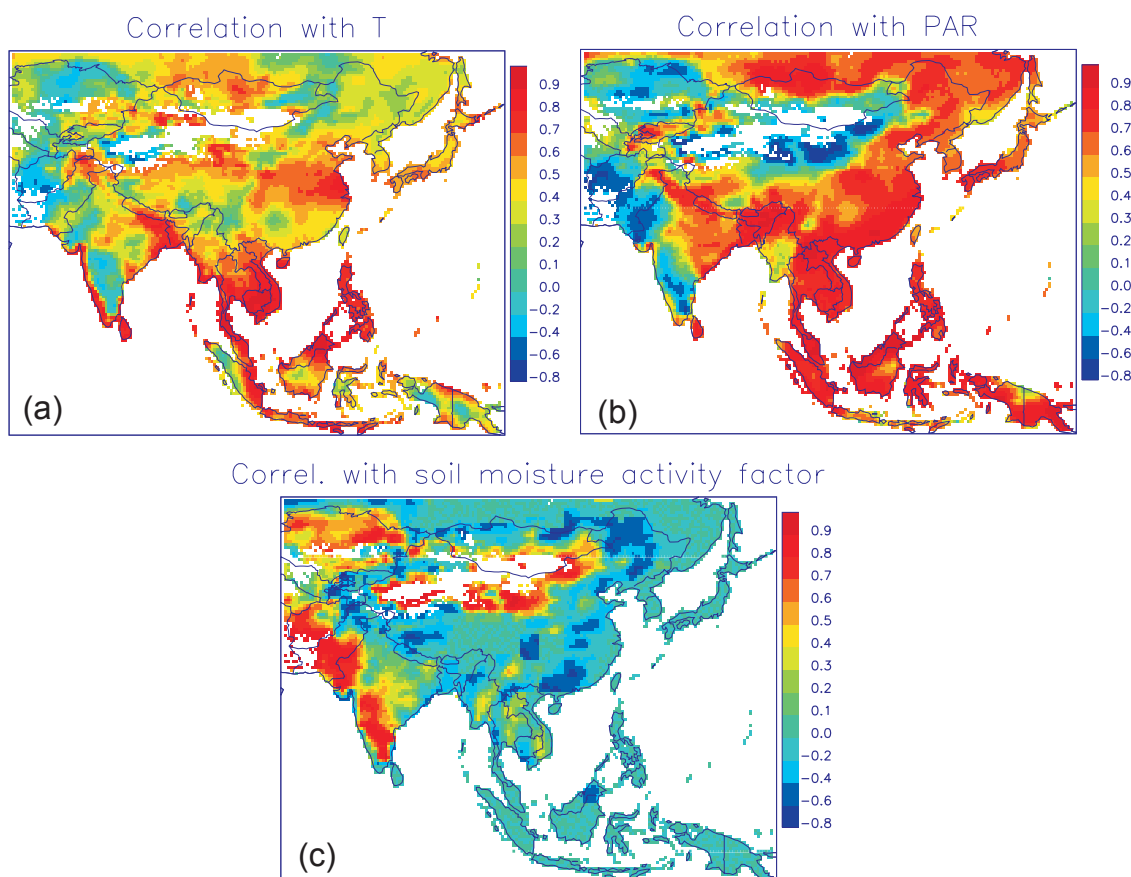
Fig. 4. Correlation coefficient between the annual isoprene emission and air temperature **(a)**, above-canopy solar radiation **(b)**, and the soil moisture stress activity factor **(c)** over 1979–2012.

Malaysia, where oil palm plantations were already considered as a major crop in the MEGAN distribution of emission factors.

The impact of solar radiation changes (simulation S4) is found to be generally small (Fig. 8). However, in India, the isoprene flux is reduced by about 8 % in 2005, as a result of the negative surface radiation anomaly (Fig. 3), whereas in China, the decrease reaches 20 %. This large decrease is due to the application of reduced downward radiation fields over China compared to the ERA-Interim data set, especially for South China, where most of the isoprene is emitted. Overall, our best bottom-up estimate (the S4 simulation) is found to be significantly lower than in the standard case (S0), with a factor of 2 reduction in the total emission, and the most drastic reductions in tropical ecosystems. The annual emission over China in 2005 is estimated at 7 Tg yr^{-1} in the S4 simulation (Table 2), within previous estimates by Klinger et al. (2002) (4.6 Tg yr^{-1}) and Li et al. (2012) (10.6 Tg yr^{-1}), and close to the value of 7.7 Tg yr^{-1} reported in Tie et al. (2006).

The seasonality of isoprene emissions estimated from the S4 scenario for 2005 is illustrated in Fig. 9. As a consequence of the generally high temperatures and solar radiation fluxes,

during summertime, this season accounts for 40 % and even 66 % of the annual emission over the studied region and over China, respectively. The fluxes are generally lower in spring and fall, totaling about 50 % over the domain, except over Myanmar and Indochina where the emission is highest during the hot-dry spring season (ca. 40 % of the annual value). In China, the flux falls to near-zero in wintertime due to the seasonal leaf drop of deciduous trees. In contrast, Indonesia and Malaysia exhibit almost no seasonality in the emitted isoprene fluxes, as displayed in Fig. 9, due to their climate remaining hot throughout the year and to the small variations in daylight duration among the seasons.

5　Country-based isoprene fluxes

The variability and trends of the annual emissions in eight Asian countries are illustrated in Fig. 10. Owing to the lack of data for solar radiation changes beyond 2005, our comparisons are limited to the period 1979–2005.

The isoprene fluxes in the standard simulation in China exhibit an upward annual trend of 0.42 % yr^{-1} in 1979–2005 (see also Fig. 6). This trend is strongly reinforced
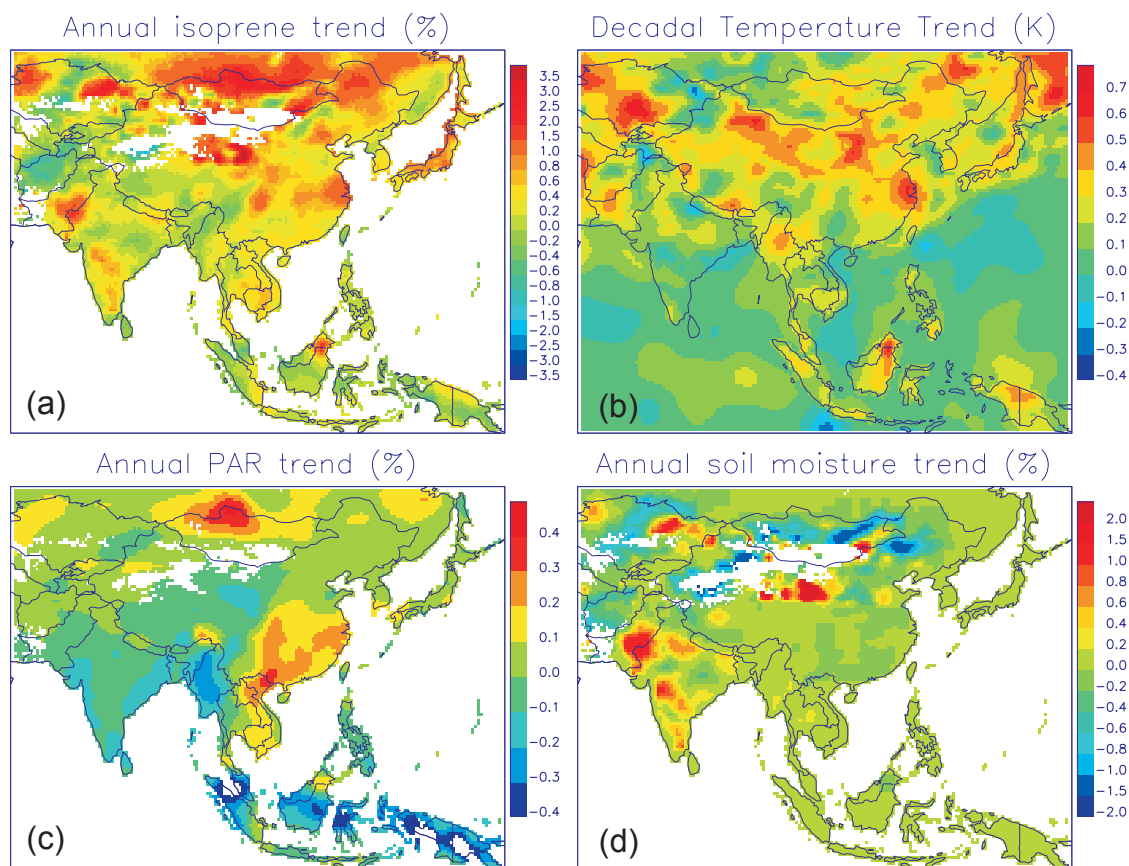
Fig. 5. Annual percentage trend in isoprene emissions derived from the S0 simulation **(a)**, decadal temperature trend **(b)**, annual percentage PAR trend **(c)** and annual percentage trend in the soil moisture activity factor **(d)** over 1979–2012 based on ERA-Interim data.

Table 2. Annual isoprene emission estimates per country simulated in the five scenarios of Table 1 for 2005. Units are Tg of isoprene. The domain extends from 9.75° S to 54.75° N and from 60.25° E to 149.75° E.

Country	S0	S1	S2	S3	S4
China	9.3	9.9	8.9	8.9	7.0
India	10.0	7.3	5.2	5.2	4.8
Indonesia	29.1	17.7	7.5	8.3	8.3
Malaysia	8.1	6.7	3.0	2.9	2.9
Thailand–Laos–Vietnam	11.5	10.7	6.0	6.0	5.7
Myanmar	6.2	5.8	2.8	2.8	2.8
Japan	0.88	0.78	0.78	0.78	0.76
Domain	90.4	71.1	41.8	42.5	39.8

when adopting the land-use changes of the S1 scenario ($0.7\% \text{ yr}^{-1}$), due to the replacement of cropland with tree plantations in China between 1979 and 2005 (Fig. 1). Higher emissions are estimated throughout the whole simulation period compared to S0, and especially after 1994. Furthermore, the updated solar radiation changes of the S4 simulation lead to an even higher emission trend ($0.78\% \text{ yr}^{-1}$) because of the solar brightening recorded in the isoprene-rich southeastern China (Fig. 3).

In addition, as a consequence of the reduced solar radiation fluxes over China (Jia et al., 2013) adopted in the S4 simulation, the emission is further reduced by about 15 % over the whole country. The interannual patterns are quite similar in all simulations; however, changes are present, e.g., the 1993–1994 peak-to-trough difference is decreased in S4 compared to S0.

In India, the fluxes undergo a reduction by about 30 % in the S1 simulation, due to the larger cropland area compared
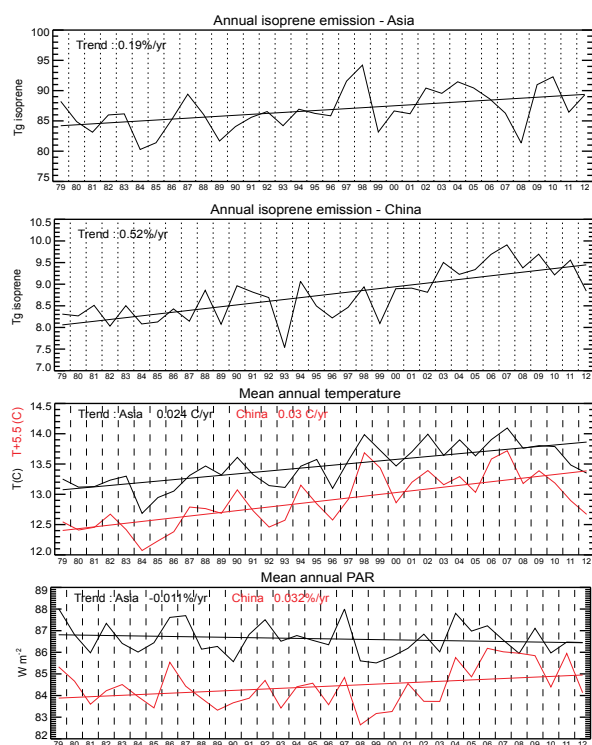
Fig. 6. Annual isoprene emissions (Tg) in the whole domain, and China (two upper panels) over 1979–2012 using the S0 simulation. Annual temperature and PAR (bottom) in Asia (black) and China (red) are shown in the two lower panels over the same period. Linear regression trends are given inset and applied over the whole simulation period.
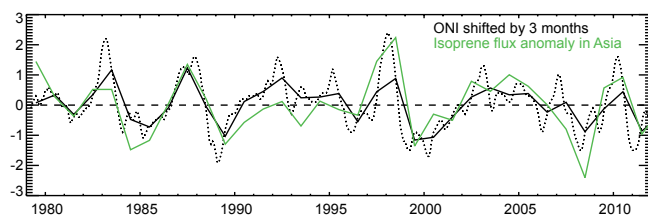

Fig. 7. Isoprene flux anomaly in Asia (green) and comparison with the Oceanic Niño Index (black) shifted by 3 months over the target period. Dotted and solid black lines correspond to monthly and annual ONI data, respectively.

to the standard MEGAN cropland distribution used in S0. These fluxes are further reduced when the emission rate for tropical forests is reduced in the S2 simulation. Whereas no significant trends are derived in the S0–S2 results, an emission trend of $-0.4\,\%\,\mathrm{yr}^{-1}$ is found in the S4 simulation, as a result of the negative trend in surface solar radiation data observed in India after 1985 (Fig. 3).

Malaysia experiences a strong emission trend in S0 ($+1.17\,\%\,\mathrm{yr}^{-1}$), attributed to the warming temperatures (up to $0.6\,^{\circ}\mathrm{C}$ per decade), and to the positive radiation trends,

especially in northeastern Borneo. The average warming rate in Malaysia exceeds by far the global warming rate of $0.6 \pm 0.2\,^{\circ}\mathrm{C}$ estimated over the past century (IPCC, 2001), in agreement with a study investigating 1961–2002 trends in surface temperature in Malaysia (Tangang et al., 2007). The emission trend in Malaysia and Indonesia is reduced from $1.17\,\%\,\mathrm{yr}^{-1}$ and $0.1\,\%\,\mathrm{yr}^{-1}$ in S0, to $0.76\,\%\,\mathrm{yr}^{-1}$ and to $-0.42\,\%\,\mathrm{yr}^{-1}$ in S1, respectively, owing to the increasing cropland fraction in these countries between 1979 and 2005 (Fig. 1). The emissions are further reduced by approximately 25 % in Indonesia due to the higher cropland fraction in S1 compared to S0, with additional reduction by a factor of approximately 2–3 in the S2 scenario as discussed in Sect. 4. Finally, accounting for the temporal evolution in oil palm plantation area (Fig. 2), leads to an enhancement of the emission trend in S3 simulation: the trend becomes strongly positive in Malaysia ($1.5\,\%\,\mathrm{yr}^{-1}$), but keeps its negative sign in Indonesia ($-0.13\,\%\,\mathrm{yr}^{-1}$).

Large modulations in the annual emissions are found in Thailand–Laos–Vietnam (Fig. 10), associated with the variability in temperature, largely driven by the El Niño Southern Oscillation. The emission trend is found to be positive throughout 1979–2005 in all simulations. However, it decreases from $0.4\,\%\,\mathrm{yr}^{-1}$ in S0 to $0.2\,\%\,\mathrm{yr}^{-1}$ in S1 due the gradually increasing cropland fraction (cf. Fig. 1). Furthermore, the emission flux is strongly reduced (a factor of 2) in the S2 scenario.

Although Japan is not a strong isoprene emitter, with an annual emission totaling less than $1\,\mathrm{Tg}$, it is worth noting the high interannual variability, mainly driven by temperature. In fact, warming rates ranging between 0.2 and $0.4\,^{\circ}\mathrm{C}$ per decade between 1979–2005 are calculated using the ECMWF fields, broadly consistent with long-term measurement records at a large number of Japanese stations between 1900 and 1996 showing a quasi-uniform upward trend in mean temperature, with estimated decadal warming rates of 0.05–$0.3\,^{\circ}\mathrm{C}$ (Yue and Hashino, 2003). The emission trends are slightly increasing across the simulations ($0.86\,\%\,\mathrm{yr}^{-1}$ in S0, $1.01\,\%\,\mathrm{yr}^{-1}$ in S1, $1.04\,\%\,\mathrm{yr}^{-1}$ in S4) owing to the influence of solar brightening recorded in Japan after 1990, as illustrated in Fig. 3.

6 Comparison with field campaign measurements

We evaluate the inventory against the tower measurements of the OP3 (Oxidant and Particle Photochemical Processes above a Southeast Asian Rainforest) project (Hewitt et al., 2010) at the Bukit Atur station in the Danum Valley region of Sabah, Malaysia (4.98° N, 117.84° E). The measurements were carried out over two four-week periods, with phase 1 (OP3-I) taking place during the months of April and May 2008 and phase 2 (OP3-III) between June and July 2008. The comparison of calculated fluxes with the measurements (Fig. 11) confirms the strong overestimation of the basal
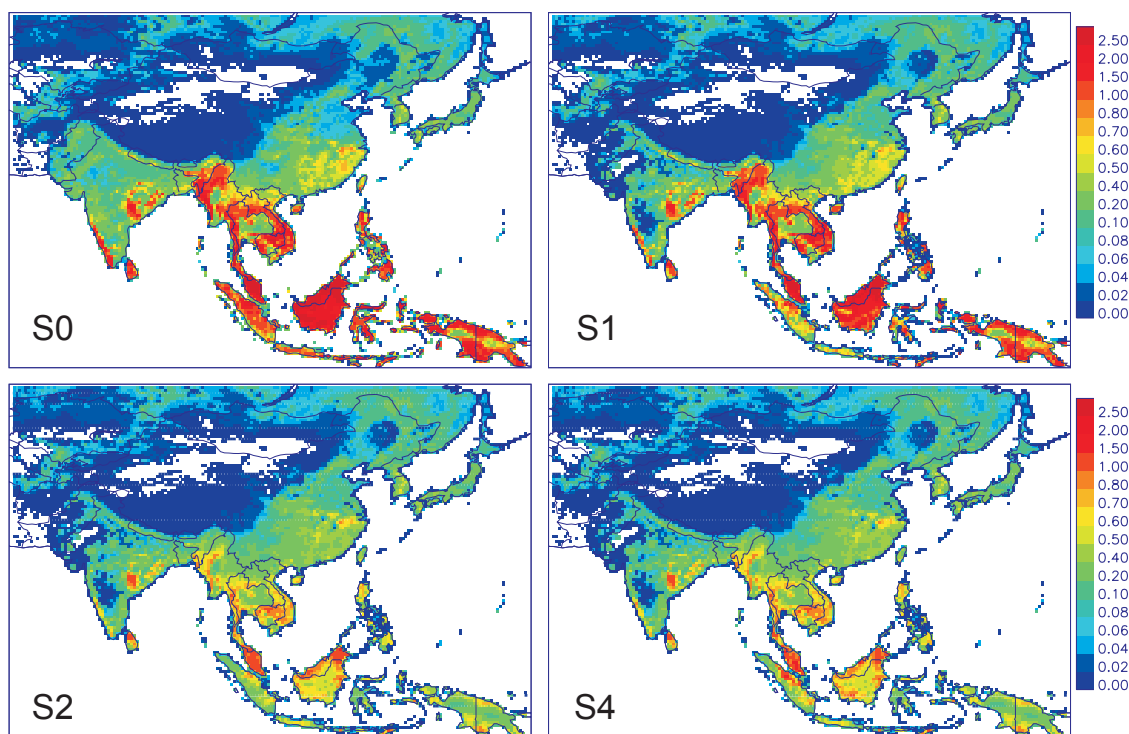
Fig. 8. Annually averaged isoprene emission rates computed in the S0, S1, S2 and S4 simulations for 2005. S1 accounts for land-use change effects, S2 also incorporates reduced emission rates from tropical forests, and S4 includes both updates in solar radiation and in the representation of oil palm in Indonesia and Malaysia (Table 1). The S4 simulation is identical to S3 over Indonesia and Malaysia.

emission rate for tropical forests in Southeast Asia (Langford et al., 2010). The average simulated fluxes in S0 are overestimated by factors of about 7 and 5 during the wet (phase 1) and dry seasons (phase 2), respectively. These larger factors compared to the factor of 4.1 inferred by Langford et al. (2010) are due to the larger average BER ($10 \, \text{mg} \, \text{m}^{-2} \, \text{h}^{-1}$) at the location of Bukit Atur in our S0 simulation compared to the basal emission rate of $6.6 \, \text{mg} \, \text{m}^{-2} \, \text{h}^{-1}$ used by Langford et al. (2010). Adopting the latter BER value in our simulations would lead to overestimation factors of 4.5 and 3.3 during the two phases, in excellent agreement with Langford et al. (2010). The factor of $\sim$2 higher emissions during the dry season compared to the wet season are only partly explained by the dependence of the emissions on temperature and radiation in the MEGAN model, since the average temperature and radiation levels were only moderately higher during phase 2 compared to phase 1 (by $0.5 \, \text{K}$ and $25 \, \%$, respectively). Changes in phenology are therefore the most likely cause of the higher apparent basal emission rate during the dry season compared with the wet season, by a factor of about 1.4 according to the model simulations.

In contrast with the seasonal variation discussed above, the emissions of isoprene (also monoterpenes) measured by eddy covariance above a tropical plantation of rubber trees (*Hevea brasiliensis*) in the Xishuangbanna Gardens (21.92° N, 101.27° E), Yunnan, South China, exhibited much higher val-

ues in the wet season than in the dry season (Baker et al., 2005). The average daytime isoprene emissions were found to be 1 and $0.15 \, \text{mgC} \, \text{m}^{-2} \, \text{s}^{-1}$ during the wet season (July 2002) and the dry season (February–March 2003), respectively, whereas our MEGAN-based inventory (S0) predicts higher emissions during the dry season ($0.64 \, \text{mgC} \, \text{m}^{-2} \, \text{s}^{-1}$) than in the wet season ($0.44 \, \text{mgC} \, \text{m}^{-2} \, \text{s}^{-1}$), due to generally lower cloudiness and higher temperatures and radiation levels during the dry season. As discussed by Baker et al. (2005), the lower dry season fluxes of monoterpenes result from the drought deciduous nature of the main monoterpene emitter, *Hevea brasiliensis*, which is however a low isoprene emitter. The very low dry season isoprene fluxes were very probably caused by extreme water stress conditions (Baker et al., 2005). The soil moisture activity factor is however equal to unity at all times in 2002/2003, based on the MEGAN parameterization (Guenther et al., 2006) using the ECMWF wilting point and soil moisture fields. In fact, the severe drought at the site in February/March 2003 is not recorded in the ERA-Interim data, which do not even show lower soil moisture content values in this period compared to other months of the year. The soil moisture activity factor is very uncertain, as it has been found to be very dependent on the choice of the soil moisture and wilting point database (Müller et al., 2008; Marais et al., 2012; Tawfik et al., 2012; Sindelarova et al., 2014): for example, the reduction in global
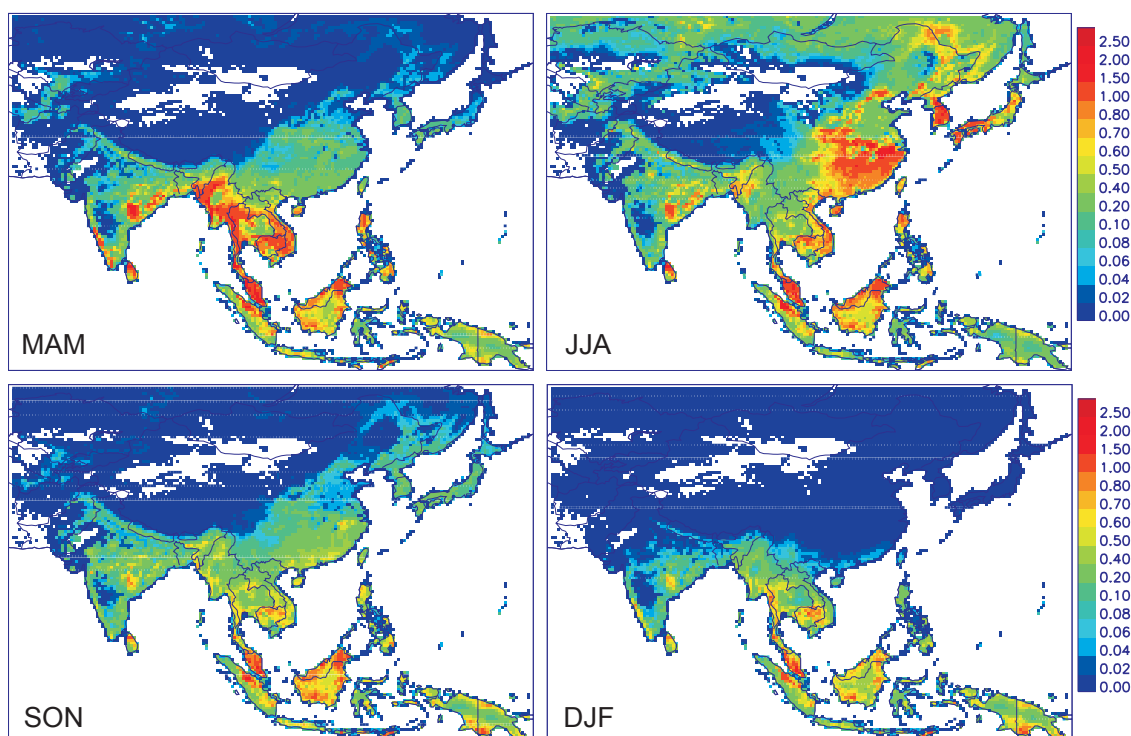
Fig. 9. Seasonal isoprene emission rates calculated by the S4 simulation in 2005 expressed in mg isoprene $m^{-2} h^{-1}$ in March-April-May (MAM), June-July-August (JJA), September-October-November (SON), and December-January-February (DJF).

annual emissions due to this activity factor ranges between 7 % (Guenther et al., 2006) and 50 % (Sindelarova et al., 2014).

7 Comparison with satellite-derived isoprene emission estimates

7.1 Setting up the inversion of HCHO columns

Formaldehyde (HCHO) is a major intermediate product in the degradation of isoprene in the atmosphere. Isoprene is found to be responsible for about 30 % of the formaldehyde formed on the global scale, but its contribution over densely vegetated continental areas can be as high as 90 % (Stavrakou et al., 2009a). HCHO vertical column abundances obtained from satellite observations have been used in a number of studies as an independent means of constraining the isoprene fluxes and possibly improving the currently available bottom-up inventories. The capabilities of HCHO columns retrieved from satellite instruments have been explored in several studies aiming to derive isoprene emission estimates over the United States (e.g., Palmer et al., 2003), over China and Southeast Asia (e.g., Fu et al., 2007), on the global scale (Stavrakou et al., 2009b), and more recently, over Africa (Marais et al., 2012). In the present study, isoprene emissions over East and South Asia are derived by adopting a

grid-based source inversion scheme (Stavrakou et al., 2009b) constrained by a new data set of HCHO columns measured by the GOME-2/MetOp-A satellite instrument between 2007 and 2012 (De Smedt et al., 2012). The settings adopted for this retrieval were optimized in order to minimize the effect of spectral interferences between HCHO and BrO, to contend with ozone absorption at high solar zenith angles, and to mitigate instrumental drifts, so as to ensure maximum consistency with HCHO columns obtained from earlier sensors (e.g., GOME and SCIAMACHY, De Smedt et al. (2012)). HCHO columns are available on the TEMIS website (http://h2co.aeronomie.be). A detailed error characterization of the columns is provided in De Smedt et al. (2012).

The source inversion is built on the IMAGESv2 (Intermediate Model of Annual and Global Evolution of Species) global chemistry-transport model run at a resolution of $2° \times 2.5°$ and resolved in 40 vertical levels from the surface to the lower stratosphere. Separate inversions are performed for each year from 2007 to 2012. Advection is driven by ERA-Interim fields (Müller and Stavrakou, 2005; Stavrakou et al., 2012, 2013). The isoprene oxidation chemistry, which recycles OH more efficiently than generally assumed in models under low NO_x conditions, follows the LIM0 mechanism (Peeters and Müller, 2010), with reduced isomerization rates of isoprene peroxy radicals based on an updated theoretical estimation (Peeters et al., 2012). Box model calculations show that accounting for the isomerization in the
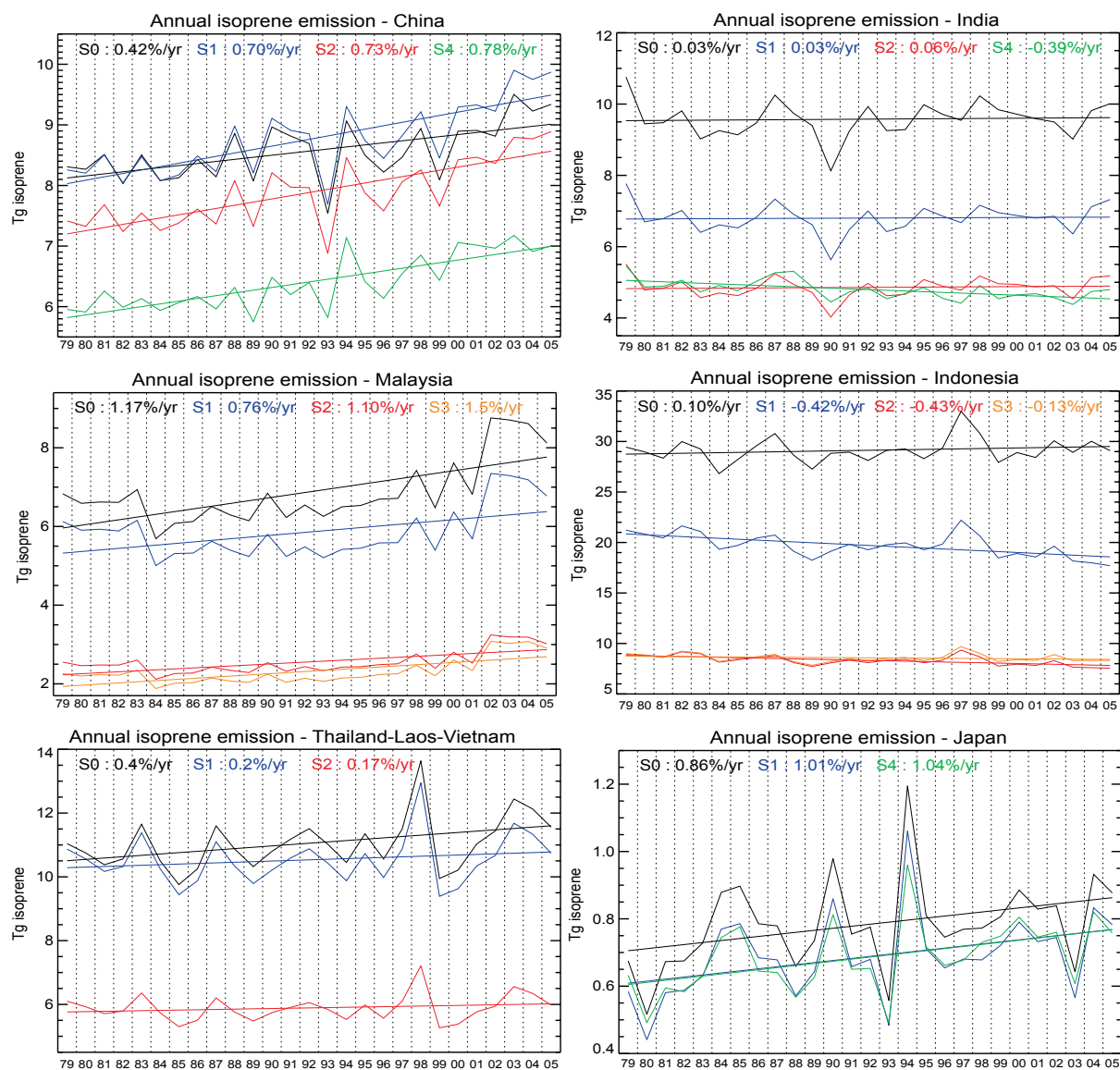
Fig. 10. Annual isoprene emission per country between 1979 and 2005. The colors denote the different simulations: S0 in black, S1 in blue, S2 in red, S3 in orange, and S4 in green (Table 1). Relative trends obtained by linear regression are given inset following the same color code. Scenarios yielding identical results are not shown, e.g., S2 and S3 over Japan.

isoprene oxidation reduces the HCHO yield from isoprene by about 10 % in both high and low NO_x regimes. Nevertheless, the isoprene degradation mechanism is far from being elucidated, especially in low NO_x conditions, and therefore remains a major source of uncertainty when mapping isoprene estimates using HCHO observations.

Anthropogenic NMVOC emissions over Asia are taken from the REASv1 inventory (Ohara et al., 2007) until 2009 and are set to 2009 values after that year. Vegetation fire emissions are obtained from GFEDv3 (van der Werf et al., 2010) until 2011 and are set to 2011 values in 2012. The biogenic emissions of isoprene are obtained by S4 for 2007–2012 (Table 1) (i) using the 2007 cropland map for 2008–

2012 and the 2010 oil palm distribution for 2011–2012, and (ii) applying only the correction factors for China from Jia et al. (2013) to all years. This data set of bottom-up emissions spanning 1979–2012 is available for use at http://tropo.aeronomie.be/models/isoprene.htm (MEGAN-ECMWF-v2).

We use monthly averaged GOME-2 HCHO columns binned onto the resolution of IMAGESv2. Observations over ocean and cloudy pixels (i.e., cloud fraction above 20 %) are filtered out. The error on the columns is taken equal to the retrieval error augmented by an absolute error of 2×10^{15} molec cm^{-2} and is generally comprised of between 30–40 %. The inversion optimizes monthly emission fluxes for three emission categories: anthropogenic, biomass burning
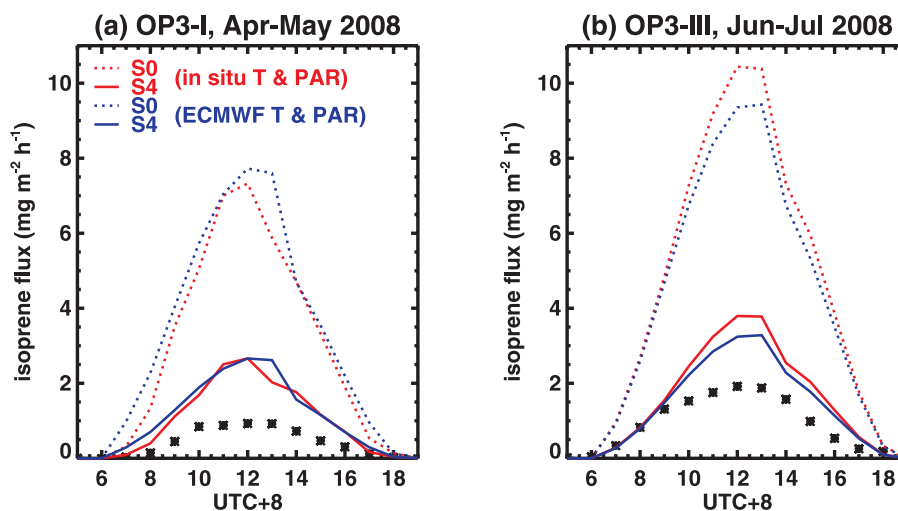
Fig. 11. Average diurnal profile of measured isoprene fluxes (black symbols) during **(a)** phase 1 and **(b)** phase 2 of the OP3 field campaigns (Langford et al., 2010) compared with calculated profiles from the S0 and S4 simulations using meteorological fields from either in situ measurements (Fig. 6b in Langford et al.) or ECMWF ERA-Interim data (Table 1).

and biogenic (isoprene and terpenes). The error correlation setup is described in Stavrakou et al. (2009b). The assumed error on the biogenic emissions is set equal to a factor of 2.5. Here we present only inferred isoprene fluxes over Asia. Further details regarding the settings as well as the global-scale results for all emission categories are beyond the scope of this study and will be presented in a forthcoming study. The GOME-2-inferred isoprene emissions are available through the GlobEmission website (http://www.globemission.eu) and described in Bauwens et al. (2013).

7.2 Top-down results

The bottom-up and top-down estimates per country and year are summarized in Table 3. The top-down estimates remain relatively close to the a priori over the entire domain, supporting the strong emission reductions of the S4 simulation over the much higher fluxes of the standard S0 scenario. Slightly higher total emissions are inferred in 2007 and 2010 compared to the other years for the whole domain, whereas lower emissions are found in 2008, in line with Fig. 6.

On a country basis, moderately lower fluxes are derived in Indonesia and Malaysia, reinforcing the evidence by Saito et al. (2008); Langford et al. (2010) that the tropical rainforests are weaker isoprene emitters in this region, and suggesting that even lower flux rates might be necessary to reproduce the formaldehyde observations in these ecosystems. On the other hand, however, the inferred enhancement by 25 % of the flux strengths in Indochina (Table 3), indicates that the isoprene rate measured during OP3 might not be representative of tropical forests over other regions like Thailand.

In China and India, the satellite-derived emissions lie close to the a priori (S4). In terms of interannual variability, the inferred isoprene fluxes in China are found to decrease from 8.6 Tg in 2007 to 6.5 Tg in 2012 (Table 3), in line with the decreasing flux trend caused by the cooling episode after 2007 (Fig. 6). In order to verify the robustness of the top-down negative trend, we conducted sensitivity inversions through 2007–2012 with isoprene emissions kept constant for all years and set to the values of 2007. Even in this case, a gradual decline in Chinese emissions is deduced after 2007, from 8.6 Tg in 2007 to 7.1 Tg in 2012, demonstrating that the top-down decline is induced by the HCHO observations, and is not due to the variability of the a priori used as input in the inversions. In a general manner, the sensitivity inversions (not shown here for the sake of simplicity) yield very similar results, in terms of both magnitude and interannual variation.

Figure 12 displays the spatial distribution of the a priori (bottom-up) isoprene emissions and the deviation from the a priori inferred by the inversion in 2008. Although the inferred updates with respect to the a priori are small when averaged over the domain, the satellite data suggest 30 % higher emissions in southeastern China, and ca. 30 % lower fluxes in central Borneo. Whereas the emission update pattern for Borneo is repeated through 2007–2012, pointing to an overestimation of isoprene rates in the bottom-up inventory for central Borneo, the inferred changes in southern China do not exhibit any systematic pattern: they are positive in 2007–2009, close to zero in 2010, and negative in 2011 and 2012. Interestingly, the inversion infers only negligible emission changes over Sabah (northern Borneo), more precisely in the region where flux measurements were performed during the OP3 campaign, indicating that the constraint on the emission provided by HCHO columns is consistent with the local canopy-
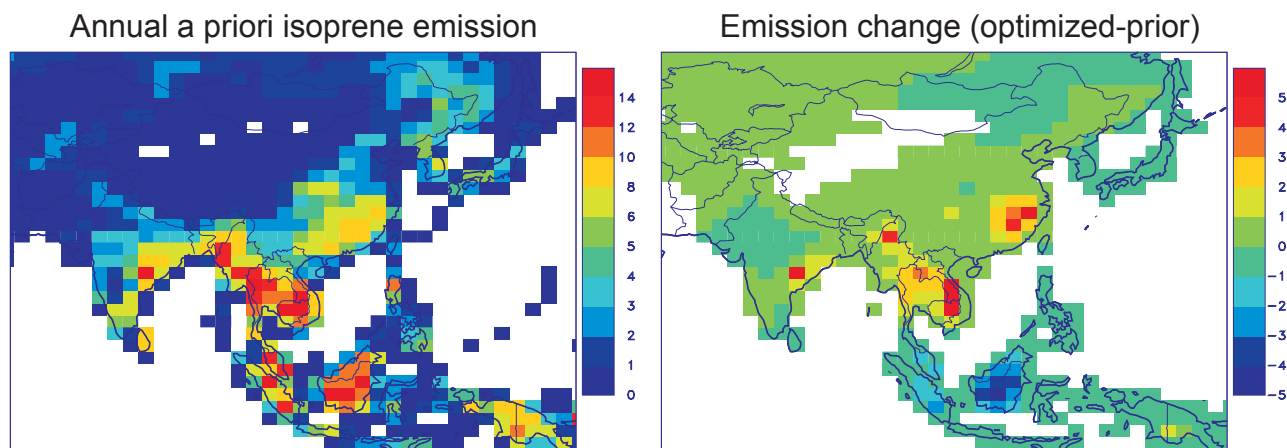
Fig. 12. Annual a priori isoprene emission in 2008 and deviation from the a priori inferred by an inversion constrained by GOME-2 HCHO columns. Units are 10^{10} molec cm^{-2} s^{-1}. The a priori inventory is obtained from the S4 simulation (cf. Sect. 7.1).

Table 3. Bottom-up (in parentheses) and top-down annual isoprene emission estimates per country and for the entire studied domain (expressed in Tg of isoprene) between 2007 and 2012. Top-down estimates are inferred by inversion of GOME-2 formaldehyde columns as explained in Sect. 7. The bottom-up estimates are obtained from the S4 simulation (cf. Sect. 7.1). The domain extends from 9.75° S to 54.75° N and from 60.25° E to 149.75° E.

Country	2007	2008	2009	2010	2011	2012
China	(7.6) 8.6	(7.2) 8.2	(7.3) 8.0	(7.0) 7.5	(7.2) 7.0	(6.7) 6.5
India	(4.9) 5.3	(4.7) 5.1	(5.0) 5.6	(5.0) 5.2	(4.9) 5.3	(4.8) 5.4
Indonesia	(7.4) 6.6	(7.0) 6.1	(8.4) 7.7	(8.0) 7.3	(8.2) 7.7	(8.4) 7.3
Malaysia	(1.7) 1.6	(1.6) 1.4	(2.1) 1.9	(2.1) 1.9	(1.9) 1.8	(1.9) 1.7
Thailand–Laos–Vietnam	(5.1) 6.6	(4.6) 6.1	(5.2) 6.3	(5.9) 7.3	(4.4) 5.9	(5.2) 5.9
Myanmar	(2.6) 3.2	(2.6) 2.9	(3.0) 3.4	(3.2) 3.5	(2.5) 2.9	(2.8) 3.2
Japan	(0.70) 0.66	(0.68) 0.64	(0.55) 0.55	(0.77) 0.74	(0.65) 0.65	(0.73) 0.70
Domain	(39.3) 43.0	(37.3) 39.4	(40.2) 42.3	(41.6) 43.2	(39.0) 40.7	(40.0) 40.3

scale flux measurements during that campaign in spite of their limited representativity at the coarse resolution of the model.

8 Conclusions

We have investigated the interannual variability of isoprene emissions in Asia between 1979 and 2012, using the MEGAN emission model combined with the MOHYCAN canopy environment model. Changes in isoprene emissions induced by the warming climate, changes in solar radiation, and the conversion of primary forests to croplands and oil palm plantations have been explored through sensitivity calculations. Furthermore, estimates of isoprene emission rates for tropical forests and oil palms suggested by recent flux observations have also been included.

Adopting MEGAN–MOHYCAN as our basis simulation (S0), we account for (i) time-dependent crop distribution, (ii) reduced emission factors for tropical forests, and (iii) distributions and trends in oil palm plantation in combination with a modified MEGAN algorithm optimized for emissions by oil palms. The S4 simulation builds upon all previous settings, and accounts further for solar radiation changes. The main results are summarized below.

– Temperature, solar radiation and soil moisture are the main drivers of interannual variability. The average warming trend over Asia (0.24 °C per decade) is the primary cause for the calculated increase in isoprene emissions over Asia, estimated at 0.2 % per year in the S0 simulation. Whereas the emission trend is higher in China (0.52 % yr^{-1} on average) it is close to zero in Indonesia and India, as a result of simultaneous increases in temperature and cloudiness. Even stronger trends (up to 3 % yr^{-1}) are found on the regional scale. The isoprene flux anomaly over the whole domain is strongly correlated ($r=0.73$) with the Oceanic Niño Index (ONI). The highest and lowest total emissions occurred in 1997–1998 (El Niño) and 2008 (La Niña), respectively.

- The model updates lead to a drastic reduction (a factor of 2) in the total emissions over the domain, primarily due to (i) lower emission rates for South Asian tropical forests, (ii) higher cropland fractions in the land-use database of Ramankutty and Foley (1999) compared to the MEGAN distribution, and (iii) lower solar radiative fluxes over China, in better agreement with ground-based observations. The largest emission reductions (factors of 2.5–3.5) are found over Indonesia and Malaysia, while the reduction in India and Indochina is lower but still important (ca. a factor of 2).

- Whereas crop abandonment and solar brightening in China are found to reinforce the emission trend ($0.72\,\%\,\mathrm{yr}^{-1}$ in the S4 simulation), pronounced solar dimming in India is responsible for the predicted decline ($-0.4\,\%$) in the emissions. Over Malaysia, the substantial warming temperatures, in combination with the rapid expansion of oil palm plantations, explain the large emission trend ($1.5\,\%\,\mathrm{yr}^{-1}$).

Comparison of our results with OP3 field measurements at Bukit Atur in Borneo confirms the overestimation of the MEGAN basal emission rate for tropical forests in Southeast Asia, as previously found by Langford et al. (2010). Moreover, the larger overestimation found during the dry season suggests a seasonal variation of the basal emission rate, with dry season values higher by 40 % compared to the wet season. An opposite pattern is observed at a tropical plantation in Yunnan (South China) with much lower dry season fluxes, presumably related to strong drought stress. This behaviour is however not reproduced by the model simulations, pointing to deficiencies in the soil moisture fields in the ERA-Interim and possibly in the MEGAN parameterization of the soil moisture stress activity factor.

Our results are partially validated by inverse modeling using formaldehyde as a proxy for VOC emissions. The GOME-2 observations largely support the evidence that tropical rainforests are weaker isoprene emitters than assumed in MEGAN, in particular over Indonesia and Malaysia. Over Indochina, the inferred emissions are 25 % higher than in the S4 inventory. Top-down results are very close to the a priori over China and India. Over China, a significant emission decline is found after 2007 ($-25\,\%$ in 5 years), consistent with the emission decrease in the bottom-up inventory resulting from the cooling trend over China beyond 2007.

The substantially lower fluxes with respect to current estimates in East and Southeast Asia strengthen the relative importance of anthropogenic emissions of volatile organic compounds in this rapidly changing region, with possibly important consequences for air pollution control strategies. It is however acknowledged that this decrease is largely due to the use of reduced isoprene rates for tropical forests, which is based on a single measurement campaign, underscoring the need for additional flux measurements above tropical forests. Nevertheless, the substantial reduction in emission factors

for all Asian tropical forests appears to be consistent with the top-down results constrained by formaldehyde observations.

References

Arneth, A., Niinemets, Ü., Pressley, S., Bäck, J., Hari, P., Karl, T., Noe, S., Prentice, I. C., Serça, D., Hickler, T., Wolf, A., and Smith, B.: Process-based estimates of terrestrial ecosystem isoprene emissions: incorporating the effects of a direct CO_2-isoprene interaction, Atmos. Chem. Phys., 7, 31–53, doi:10.5194/acp-7-31-2007, 2007.

Baker, B., Bai, J.-H., Johnson, C., Cai, Z.-T., Li, Q. J., Wang, Y.-F., Guenther, A., Greenberg, J., Klinger, L., Geron, C., and Rasmussen, R.: Wet and dry season ecosystem fluxes of isoprene and monoterpenes from a southeast Asian secondary forest and rubber tree plantation, Atmos. Environ., 39, 381–390, 2005.

Bauwens, M., Stavrakou, T., Müller, J.-F., De Smedt, I., and Van Roozendael, M.: Satellite-based isoprene emission estimates (2007–2012) from the GlobEmission project, Proceedings of the ACCENT-Plus Symposium, Atmospheric Composition Change-Policy Support and Science, Urbino, 17–20 September, 2013.

Claeys, M., Graham, B., Vas, G., Wang, W., Vermeylen, R., Pashynska, V., Cafmeyer, J., Guyon, P., Andreae, M. O., Artaxo, P., and Maenhaut, W.: Formation of secondary organic aerosols through photooxidation of isoprene, Science, 303, 1173–1176, 2004.

Crounse, J. D., Paulot, F., Kjaergaard, H. G., and Wennberg, P. O.: Peroxy radical isomerization in isoprene oxidation, Phys. Chem. Chem. Phys., 13, 13607–13613, 2011.

De Smedt, I., Van Roozendael, M., Stavrakou, T., Müller, J.-F., Lerot, C., Theys, N., Valks, P., Hao, N., and van der A, R.: Improved retrieval of global tropospheric formaldehyde columns from GOME-2/MetOp-A addressing noise reduction and instrumental degradation issues, Atmos. Meas. Tech., 5, 2933–2949, doi:10.5194/amt-5-2933-2012, 2012.

Fowler, D., Nemitz, E., Misztal, P., Di Marco, C., Skiba, U., Ryder, J., Helfter, C., Neil Cape, J., Owen, S., Dorsey, J., Gallagher, M. W., Coyle, M., Philips, G., Davison, B., Langford, B., MacKenzie, R., Muller, J., Siong, J., Dari-Salisburgo, C., Di Carlo, P., Aruffo, E., Giammaria, F., Pyle, J., and Hewitt, C. N.: Effects of land use on surface-atmosphere exchanges of trace gases and energy in Borneo: comparing fluxes over oil palm plantations and a rainforest, Phil. Trans. R. Soc. B, 366, 3196–3209, doi:10.1098/rstb.2011.0055, 2011.

Fu, T. M., Jacob, D. J., Palmer, P. I., Chance, K., Wang, Y. X., Barletta, B., Blake, D. R., Stanton, J. C., and Pilling, M. J.: Space-based formaldehyde measurements as constraints on volatile organic compound emissions in east and south Asia and implications for ozone, J. Geophys. Res., 112, D06312, doi:10.1029/2006JD007853, 2007.

Geron, C., Owen, S., Guenther, A., Greenberg, J., Rasmussen, R., Bai, J. H., Li, Q.-J., and Baker, B.: Volatile organic compounds from vegetation in southern Yunnan Province, China: Emission rates and some potentail regional implications, Atmos. Environ., 40, 1759–1773, 2006.

Goudriaan, J. and van Laar, H.: Modelling potential crop growth processes, Textbook with Exercises, Kluwer Academic Publishers, Dordrecht, The Netherlands, 1994.

Guenther, A., Karl, T., Harley, P., Wiedinmyer, C., Palmer, P. I., and Geron, C.: Estimates of global terrestrial isoprene emissions using MEGAN (Model of Emissions of Gases and Aerosols from Nature), Atmos. Chem. Phys., 6, 3181–3210, doi:10.5194/acp-6-3181-2006, 2006.

Guenther, A. B., Jiang, X., Heald, C. L., Sakulyanontvittaya, T., Duhl, T., Emmons, L. K., and Wang, X.: The Model of Emissions of Gases and Aerosols from Nature version 2.1 (MEGAN2.1): an extended and updated framework for modeling biogenic emissions, Geosci. Model Dev., 5, 1471–1492, doi:10.5194/gmd-5-1471-2012, 2012.

Heald, C. L., Wilkinson, M. J., Monson, R. K., Alo, C. A., Wang, G., and Guenther, A.: Response of isoprene emission to ambient CO_2 changes and implications for global budgets, Glob. Change Biol., 15, 1127–1140, doi:10.1111/j.1365-2486.2008.01802.x, 2009.

Hewitt, C. N., Lee, J. D., MacKenzie, A. R., Barkley, M. P., Carslaw, N., Carver, G. D., Chappell, N. A., Coe, H., Collier, C., Commane, R., Davies, F., Davison, B., DiCarlo, P., Di Marco, C. F., Dorsey, J. R., Edwards, P. M., Evans, M. J., Fowler, D., Furneaux, K. L., Gallagher, M., Guenther, A., Heard, D. E., Helfter, C., Hopkins, J., Ingham, T., Irwin, M., Jones, C., Karunaharan, A., Langford, B., Lewis, A. C., Lim, S. F., MacDonald, S. M., Mahajan, A. S., Malpass, S., McFiggans, G., Mills, G., Misztal, P., Moller, S., Monks, P. S., Nemitz, E., Nicolas-Perea, V., Oetjen, H., Oram, D. E., Palmer, P. I., Phillips, G. J., Pike, R., Plane, J. M. C., Pugh, T., Pyle, J. A., Reeves, C. E., Robinson, N. H., Stewart, D., Stone, D., Whalley, L. K., and Yin, X.: Overview: oxidant and particle photochemical processes above a south-east Asian tropical rainforest (the OP3 project): introduction, rationale, location characteristics and tools, Atmos. Chem. Phys., 10, 169–199, doi:10.5194/acp-10-169-2010, 2010.

Hewitt, C. N., Ashworth, K., Boynard, A., Guenther, A., Langford, B., MacKenzie, A. R., Misztal, P. K., Nemitz, E., Owen, S. M., Possell, M., Pugh, T. A. M., Ryan, A. C., and Wild, O.: Ground-level ozone influenced by circadian control of isoprene emissions, Nature Geosci., 4, 671–674, doi:10.1038/ngeo1271, 2011.

IPCC: Climate Change, The scientific basis. Contribution of Working group I to the Third Assessment Report of the Intergovernamental panel on Climate Change, Cambridge, UK, Cambridge University press, 2001.

Jia, B., Xie, Z., Dai, A., Shi, C., and Chen, F.: Evaluation of satellite and reanalysis products of downward surface solar radiation over East Asia: spatial and seasonal variations, J. Geophys. Res., 118, 3431–3446, doi:10.1002/jgrd.50353, 2013.

Klinger, L. F., Li, Q.-J., Guenther, A., Greenberg, J., Baker, B., and Bai, J.: Assessment of volatile organic compound emissions from ecosystems of China, J. Geophys. Res., 107, 4603, doi:10.1029/2001JD001076, 2002.

Koh, L. P., Miettinen, J., Liew, S. C., and Ghazoul, J.: Remotely sensed evidence of tropical peatland conversion to oil palm, P. Natl. Acad. Sci., 108, 5127–5132, doi:10.1073/pnas.1018776108, 2011.

Kurokawa, J., Ohara, T., Morikawa, T., Hanayama, S., Janssens-Maenhout, G., Fukui, T., Kawashima, K., and Akimoto, H.: Emissions of air pollutants and greenhouse gases over Asian regions during 2000–2008: Regional Emission inventory in ASia (REAS) version 2, Atmos. Chem. Phys., 13, 11019–11058, doi:10.5194/acp-13-11019-2013, 2013.

Langford, B., Misztal, P. K., Nemitz, E., Davison, B., Helfter, C., Pugh, T. A. M., MacKenzie, A. R., Lim, S. F., and Hewitt, C. N.: Fluxes and concentrations of volatile organic compounds from a South-East Asian tropical rainforest, Atmos. Chem. Phys., 10, 8391–8412, doi:10.5194/acp-10-8391-2010, 2010.

Lathière, J., Hauglustaine, D. A., Friend, A. D., De Noblet-Ducoudré, N., Viovy, N., and Folberth, G. A.: Impact of climate variability and land use changes on global biogenic volatile organic compound emissions, Atmos. Chem. Phys., 6, 2129–2146, doi:10.5194/acp-6-2129-2006, 2006.

Lathière, J., Hewitt, C. N., and Beerling, D. J.: Sensitivity of isoprene emissions from the terrestrial biosphere to 20th century changes in atmospheric CO_2 concentration, climate, and land use, Global Biogeochem. Cy., 24, GB1004, doi:10.1029/2009GB003548, 2010.

Lelieveld, J., Butler, T. M., Crowley, J. N., Dillon, T. J., Fischer, H., Ganzeveld, L., Harder, H., Lawrence, M. G., Martinez, M., Taraborrelli, D., and Williams, J.: Atmospheric oxidation capacity sustained by a tropical forest, Nature, 452, 737–740, 2008.

Leuning, R., Kelliher, F., De Purry, D., and Schulze, E.-D.: Leaf nitrogen, photosynthesis, conductance and transpiration: scaling from leaves to canopies, Plant Cell Environ., 1195, 1183–1200, 1995.

Li, M., Huang, X., Li, J., and Song, Y.: Estimation of biogenic volatile organic compound (BVOC) emissions from the terrestrial ecosystem in China using real-time remote sensing data, Atmos. Chem. Phys. Discuss., 12, 6551–6592, doi:10.5194/acpd-12-6551-2012, 2012.

Liu, B., Xu, M., Henderson, M., Qi, Y., and Li, Y.: Taking China's temperature: daily range, warming trends, and regional variations, 1955–2000, J. Climate, 17, 4453–4462, 2004.

Madronich, S. and Flocke, S.: The role of solar radiation in atmospheric chemistry, in: Handbook of Environmental Chemistry, edited by: Boule, P., Springer Verlag, Heidelberg, 1–26, 1998.

Marais, E. A., Jacob, D. J., Kurosu, T. P., Chance, K., Murphy, J. G., Reeves, C., Mills, G., Casadio, S., Millet, D. B., Barkley, M. P., Paulot, F., and Mao, J.: Isoprene emissions in Africa inferred from OMI observations of formaldehyde columns, Atmos. Chem. Phys., 12, 6219–6235, doi:10.5194/acp-12-6219-2012, 2012.

Miettinen, J., Shi, C., Tan, W. J., and Liew, S. C.: 2010 land cover map of insular South East Asia in 250-m spatial resolution, Remote Sens. Lett., 3, 11–20, 2012a.

Miettinen, J., Hooijer, A., Tollenaar, D., Page, S., Malins, C., Vernimmen, R., Shi, C., and Liew, S. C.: Historical Analysis and projection of oil palm plantation expansion on peatland in Southeast Asia, White Paper 17, The International Council on Clean Transportation, www.theicct.org, February 2012b.

Misztal, P. K., Nemitz, E., Langford, B., Di Marco, C. F., Phillips, G. J., Hewitt, C. N., MacKenzie, A. R., Owen, S. M., Fowler, D., Heal, M. R., and Cape, J. N.: Direct ecosystem fluxes of volatile organic compounds from oil palms in South-East Asia, Atmos. Chem. Phys., 11, 8995–9017, doi:10.5194/acp-11-8995-2011, 2011.

Müller, J.-F. and Stavrakou, T.: Inversion of CO and NO_x emissions using the adjoint of the IMAGES model, Atmos. Chem. Phys., 5, 1157–1186, doi:10.5194/acp-5-1157-2005, 2005.

Müller, J.-F., Stavrakou, T., Wallens, S., De Smedt, I., Van Roozendael, M., Potosnak, M. J., Rinne, J., Munger, B., Goldstein, A., and Guenther, A. B.: Global isoprene emissions estimated using MEGAN, ECMWF analyses and a detailed canopy environment model, Atmos. Chem. Phys., 8, 1329–1341, doi:10.5194/acp-8-1329-2008, 2008.

Naik, V., Delire, C., and Wuebbles, D. J.: Sensitivity of global biogenic isoprenoid emissions to climate variability and atmospheric CO_2, J. Geophys. Res., 109, D06301, doi:10.1029/2003JD004236, 2004.

Norris, J. R. and Wild, M.: Trends in aerosol radiative effects over China and Japan inferred from observed cloud cover, solar "dimming" and solar "brightening", J. Geophys. Res., 114, D00D15, doi:10.1029/2008JD011378, 2009.

Ohara, T., Akimoto, H., Kurokawa, J., Horii, N., Yamaji, K., Yan, X., and Hayasaka, T.: An Asian emission inventory of anthropogenic emission sources for the period 1980–2020, Atmos. Chem. Phys., 7, 4419–4444, doi:10.5194/acp-7-4419-2007, 2007.

Pacifico, F., Harrison, S. P., Jones, C. D., Arneth, A., Sitch, S., Weedon, G. P., Barkley, M. P., Palmer, P. I., Serça, D., Potosnak, M., Fu, T.-M., Goldstein, A., Bai, J., and Schurgers, G.: Evaluation of a photosynthesis-based biogenic isoprene emission scheme in JULES and simulation of isoprene emissions under present-day climate conditions, Atmos. Chem. Phys., 11, 4371–4389, doi:10.5194/acp-11-4371-2011, 2011.

Padma Kumari, B., A. L. Londhe, S. Daniel, and D. B. Jadhav: Observational evidence of solar dimming: offsetting surface warming over India, Geophys. Res. Lett., 34, L21810, doi:10.1029/2007GL031133, 2007.

Palmer, P., Jacob, D. J., Fiore, A. M., and Martin, R. V.: Mapping isoprene emissions over North America using formaldehyde observations from space, J. Geophys. Res., 108, 4180, doi:10.1029/2002JD002153, 2003.

Peeters, J. and Müller, J.-F.: HO_x radical regeneration in isoprene oxidation via peroxy radical isomersations, II: Experimental evidence and global impact, Phys. Chem. Chem. Phys., 12, 14227–14235, doi:10.1039/C0CP00811G, 2010.

Peeters, J., Nguyen, S. V., Nguyen, T. L., Stavrakou, T., and Müller, J.-F.: Hydroxyl radical regeneration in isoprene oxidation: the upgraded mechanism LIM1, AGU Fall Meeting, San Francisco, 2012.

Ramanathan, V. and Carmichael, G.: Global and regional climate changes due to black carbon, Nature Geosci., 1, 221–227, 2008.

Ramankutty, N. and Foley, J. A.: Estimating historical changes in global land cover: croplands from 1700 to 1992, Global Biogeochem. Cy., 13, 997–1027, 1999.

Richter, A., Burrows, J. P., Nüss, H., Granier, C., and Niemeier, U.: Increase in tropospheric nitrogen dioxide over China observed from space, Nature, 437, 129–132, 2005.

Saito, T., Yokouchi, Y., Kosugi, Y., Tani, M., Philip, E., and Okuda, T.: Methyl chloride and isoprene emissions from tropical rain forest in Southeast Asia, Geophys. Res. Lett., 35, L19812, doi:10.1029/2008GL035241, 2008.

Sindelarova, K., Granier, C., Bouarar, I., Guenther, A., Tilmes, S., Stavrakou, T., Müller, J.-F., Kuhn, U., Stefani, P., and Knorr, W.: Global dataset of biogenic VOC emissions calculated by the MEGAN model over the last 30 years, Atmos. Chem. Phys. Discuss., 14, 10725–10788, doi:10.5194/acpd-14-10725-2014, 2014.

Stavrakou, T., Müller, J.-F., Boersma, K. F., De Smedt, I., and van der A, R. J.: Assessing the distribution and growth rates of NO_x emission sources by inverting a 10-year record of NO_2 satellite columns, Geophys. Res. Lett., 35, L10801, doi:10.1029/2008GL033521, 2008.

Stavrakou, T., Müller, J.-F., De Smedt, I., Van Roozendael, M., van der Werf, G. R., Giglio, L., and Guenther, A.: Evaluating the performance of pyrogenic and biogenic emission inventories against one decade of space-based formaldehyde columns, Atmos. Chem. Phys., 9, 1037–1060, doi:10.5194/acp-9-1037-2009, 2009a.

Stavrakou, T., Müller, J.-F., De Smedt, I., Van Roozendael, M., van der Werf, G. R., Giglio, L., and Guenther, A.: Global emissions of non-methane hydrocarbons deduced from SCIAMACHY formaldehyde columns through 2003–2006, Atmos. Chem. Phys., 9, 3663–3679, doi:10.5194/acp-9-3663-2009, 2009b.

Stavrakou, T., Müller, J.-F., Peeters, J., Razavi, A., Clarisse, L., Clerbaux, C., Coheur, P.-F., Hurtmans, D., De Mazière, M., Vigouroux, C., Deutscher, N. M., Griffith, D. W. T., Jones, N., and Paton-Walsh, C.: Satellite evidence for a large source of formic acid from boreal and tropical forests, Nature Geosci., 5, 26–30, doi:10.1038/ngeo1354, 2012.

Stavrakou, T., Müller, J.-F., Boersma, K. F., van der A, R. J., Kurokawa, J., Ohara, T., and Zhang, Q.: Key chemical NO_x sink uncertainties and how they influence top-down emissions of nitrogen oxides, Atmos. Chem. Phys., 13, 9057–9082, doi:10.5194/acp-13-9057-2013, 2013.

Steiner, A., Luo, C., Huang, Y., and Chameides, W. L.: Past and present-day biogenic volatile organic compound emissions in East Asia, Atmos. Environ., 36, 4895–4905, 2002.

Tanaka, K., Kim, H.-J., Saito, K., Takahashi, H. G., Watanabe, M., Yokohata, T., Kimoto, M., Takata, K., and Yasunari, T.: How have both cultivation and warming influenced annual global isoprene and monoterpene emissions since the preindustrial era?, Atmos. Chem. Phys., 12, 9703–9718, doi:10.5194/acp-12-9703-2012, 2012.

Tangang, F. T., Juneng, L., and Ahmad, S.: Trend and interannual variability of temperature in Malaysia: 1961–2002, Theor. Appl. Climatol., 89, 127–141, 2007.

Tawfik, A. B., Stöckli, R., Goldstein, A., Pressley, S., and Steiner, A. L.: Quantifying the contribution of environmental factors to isoprene flux interannual variability, Atmos. Environ., 54, 216–224, 2012.

Tie, X., Li, G., Ying, Z., Guenther, A., and Madronich, S.: Biogenic emissions of isoprenoids and NO in China and comparison to anthropogenic emissions, Sci. Total Environ., 371, 238–251, doi:10.1016/j.scitotenv.2006.06.025, 2006.

van der Werf, G. R., Randerson, J. T., Giglio, L., Collatz, G. J., Mu, M., Kasibhatla, P. S., Morton, D. C., DeFries, R. S., Jin, Y., and

van Leeuwen, T. T.: Global fire emissions and the contribution of deforestation, savanna, forest, agricultural, and peat fires (1997–2009), Atmos. Chem. Phys., 10, 11707–11735, doi:10.5194/acp-10-11707-2010, 2010.

Wild, M.: Global dimming and brightening: A review, J. Geophys. Res., 114, D00D16, doi:10.1029/2008JD011470, 2009a.

Wild, M.: Enlightening Global Dimming and Brightening, B. Am. Meteor. Soc., 93, 27–37, doi:10.1175/BAMS-D-11-00074.1, 2012.

Wild, M. and Schmucki, E.: Assessment of global dimming and brightening in IPCC-AR4/ CMIP3 models and ERA40, Clim. Dyn., 37, 1671–1688, doi:10.1007/s00382-010-0939-3, 2010.

Wild, M., Trüssel, B., Ohmura, A., Long, C. N., König-Langlo, G., Dutton, E. G., and Tsvetkov, A.: Global dimming and brightening: An update beyond 2000, J. Geophys. Res., 114, D00D13, doi:10.1029/2008JD011382, 2009.

Wu, S., Mickley, L. J., Kaplan, J. O., and Jacob, D. J.: Impacts of changes in land use and land cover on atmospheric chemistry and air quality over the 21st century, Atmos. Chem. Phys., 12, 1597–1609, doi:10.5194/acp-12-1597-2012, 2012.

Xia, X.: A closer looking at dimming and brightening in China during 1961–2005, Ann. Geophys., 28, 1121–1132, doi:10.5194/angeo-28-1121-2010, 2010.

Yue, S. and Hashino, M.: Temperature trends in Japan: 1900–1996, Theor. Appl. Climatol., 75, 15–27, doi:10.1007/s00704-002-0717-1, 2003.